Glycobiology, 2015, vol. 25, no. 12, 1392–1409
doi: 10.1093/glycob/cwv046
Advance Access Publication Date: 7 July 2015
Original Article

OXFORD

Cell Biology

Cell surface glycan engineering of neural stem cells augments neurotropism and improves recovery in a murine model of multiple sclerosis

Jasmeen S Merzaban[2,5,6,†], Jaime Imitola[4,7,†], Sarah C Starossom[4,8], Bing Zhu[4], Yue Wang[4], Jack Lee[2], Amal J Ali[5], Marta Olah[4], Ayman F Abuelela[5], Samia J Khoury[4,9,‡], and Robert Sackstein[1,2,3,‡]

[2]Department of Dermatology, [3]Department of Medicine, Harvard Skin Disease Research Center, and [4]Department of Neurology, Center for Neurologic Diseases, Brigham and Women's Hospital, Harvard Medical School, Boston, MA 02115, USA, and [5]Division of Biological and Environmental Sciences and Engineering (BESE), King Abdullah University of Science and Technology (KAUST), Thuwal 23955-6900, Saudi Arabia

[1]To whom correspondence should be addressed: Tel: +617-525-5601; Fax: +617-525-5571; e-mail: rsackstein@partners.org

[6]Present address: King Abdullah University of Science and Technology (KAUST), Division of Biological and Environmental Sciences and Engineering (BESE), Thuwal 23955-6900, Saudi Arabia.
[7]Present address: Laboratory for Neural Stem Cells and Functional Neurogenetics, Division of Neuroimmunology and Multiple Sclerosis, Departments of Neurology and Neuroscience, The Ohio State University Wexner Medical Center, Biomedical Research Tower, Room 688. 460 W. 12th Avenue Columbus, Ohio 43210, USA.
[8]Present address: Institute for Medical Immunology, Charite University Medicine Berlin, Berlin, Germany.
[9]Present address: Abu Haidar Neuroscience Institute, American University of Beirut Medical Center, Beirut, Lebanon.
[†]These authors share first authorship.
[‡]These authors contributed as co-senior authors.

Received 9 October 2014; Revised 17 June 2015; Accepted 2 July 2015

Abstract

Neural stem cell (NSC)-based therapies offer potential for neural repair in central nervous system (CNS) inflammatory and degenerative disorders. Typically, these conditions present with multifocal CNS lesions making it impractical to inject NSCs locally, thus mandating optimization of vascular delivery of the cells to involved sites. Here, we analyzed NSCs for expression of molecular effectors of cell migration and found that these cells are natively devoid of E-selectin ligands. Using glycosyltransferase-programmed stereosubstitution (GPS), we glycan engineered the cell surface of NSCs ("GPS-NSCs") with resultant enforced expression of the potent E-selectin ligand HCELL (hematopoietic cell E-/L-selectin ligand) and of an E-selectin-binding glycoform of neural cell adhesion molecule ("NCAM-E"). Following intravenous (i.v.) injection, short-term homing studies demonstrated that, compared with buffer-treated (control) NSCs, GPS-NSCs showed greater neurotropism. Administration of GPS-NSC significantly attenuated the clinical course of experimental autoimmune encephalomyelitis (EAE), with markedly decreased inflammation and improved oligodendroglial and axonal integrity, but without evidence of long-term stem cell engraftment. Notably, this effect of NSC is not a universal property of adult stem cells, as administration of GPS-engineered mouse hematopoietic stem/progenitor cells did not improve EAE clinical course. These findings highlight the utility of cell surface glycan engineering to boost stem cell delivery in neuroinflammatory conditions and

indicate that, despite the use of a neural tissue-specific progenitor cell population, neural repair in EAE results from endogenous repair and not from direct, NSC-derived cell replacement.

Key words: exofucosylation, glycan engineering, HCELL, multiple sclerosis, neural stem cell

Introduction

Nature has developed an extremely efficient mechanism to deliver circulating cells to sites of inflammation and injury. This process is controlled by a highly ordered cascade of molecular interactions (Butcher 1991; Springer 1994; Sackstein 2005). The first essential event in cell recruitment involves shear-resistant adhesion of flowing cells on the endothelial surface, a process most efficiently mediated by selectins, a family of three Ca^{2+}-dependent lectins (comprised of E-, P- and L-selectins), binding to their respective counter-receptors. These interactions initially tether the cell to the vessel wall and, in the context of vascular shear flow, cause the cell to roll along the endothelial surface at velocities below that of the prevailing hemodynamic stream (Step 1). This process facilitates engagement of specific cell-borne chemokine receptors to pertinent chemokines present in the perivascular areas, thereby triggering inside-out signal transduction events leading to increased adhesiveness of integrin family members (Step 2). Adhesive interactions between the activated cell integrins and their cognate endothelial cell counter-receptors then lead to arrest of rolling and firm adhesion of the cell to the vessel wall (Step 3), and, ultimately, transendothelial migration (extravasation, Step 4).

In multiple sclerosis (MS), and in its animal model, experimental autoimmune encephalomyelitis (EAE), recruitment of immunologic effectors, is mediated by the upregulation of the vascular selectins, E- and P-selectins. E- and P-selectins are expressed on brain endothelium after in vivo activation with lipopolysaccharide or tumor necrosis factor-α (TNF-α); however, in murine EAE, P-selectin is expressed only transiently (Piccio et al. 2002). Notably, E-selectin is expressed throughout the inflammatory period with a patchy distribution at sites where vessels branch, suggesting the existence of preferential recruitment areas (Piccio et al. 2002). E-selectin is also characteristically found in vessels from acute plaques in MS patients (Washington et al. 1994; Lee and Benveniste 1999). These findings suggest that E-selectin plays a dominant role in the recruitment of circulating cells to the brain in inflammatory diseases.

All three selectins bind to specialized carbohydrate determinants, comprised of sialofucosylations containing an α(2,3)-linked sialic acid substitution on galactose, and an α(1,3)-linked fucose modification on *N*-acetylglucosamine, prototypically displayed as the terminal tetrasaccharide sialyl Lewis X (sLe^x) (Polley et al. 1991; Sackstein 2005). This structure, also known as "CD15s", may be displayed on either a protein scaffold (i.e., a glycoprotein) or a lipid scaffold (i.e., a glycolipid) and is recognized by a monoclonal antibody (mAb) such as CSLEX-1 and HECA-452 (Alon et al. 1995; Fuhlbrigge et al. 1997; Dimitroff et al. 2001; Gadhoum and Sackstein 2008; Merzaban et al. 2011; AbuSamra et al. 2015). Although additional structural modifications principally involving sulfation increase binding affinity of P- and L-selectins to sLe^x, no such modifications are needed for optimal binding of E-selectin (Leppanen et al. 2000; Rosen 2004).

Neural stem cell (NSC)-based therapy has generated great hope for halting and/or reversing disease progression in central nervous system (CNS) inflammatory and/or degenerative diseases (Ben-Hur et al. 2003; Pluchino et al. 2003, 2005; Imitola, Raddassi, et al. 2004; Einstein et al. 2006, 2007; Ziv et al. 2006; Lee et al. 2008). It is well known that NSCs express Step 2 and Step 3/4 effectors, such as CXCR4 (Flax et al. 1998; Bezzi et al. 2001; Imitola, Raddassi, et al. 2004) and VLA-4 (Pluchino et al. 2005; Rampon et al. 2008), respectively, but there are no data on whether NSCs natively express Step 1 effectors. Accordingly, we examined expression of Step 1 effectors on mouse NSCs and found that these cells are conspicuously devoid of Step 1 effectors, in particular, E-selectin ligands. Using the EAE model, we analyzed whether enforced E-selectin ligand activity via cell surface glycan engineering would impact migration of administered NSCs and, more importantly, the therapeutic effect(s) of administered cells. To this end, we utilized a technology called glycosyltransferase-programmed stereosubstitution (GPS) to create relevant selectin-binding glycan determinants on the cell surface (Sackstein et al. 2008). We report here that GPS enforces expression of E-selectin ligands on NSCs by modifying glycans of two NSC membrane glycoproteins, CD44 and of neural cell adhesion molecule (NCAM), creating the E-selectin ligands HCELL (hematopoietic cell E-/L-selectin ligand) and E-selectin-binding glycoform of NCAM (NCAM-E), respectively. Glycoengineering of NSC E-selectin ligand activity resulted in increased neurotropism and yielded improved clinical outcome in EAE in the absence of detectable long-term engraftment, indicating that these tissue-specific stem cells engendered a repair effect, not a direct cell replacement effect. Importantly, this beneficial effect is not a universal property of adult stem cells, as administration of GPS-engineered mouse hematopoietic stem/progenitor cells (HSPCs) did not improve EAE clinical course. These findings have profound clinical implications in providing the first direct evidence that cell surface glycoengineering to create effectors of cell migration can improve the efficacy of stem cell-based therapeutics and also provide new perspectives on the use of NSCs in the treatment of neuroinflammatory diseases.

Results

Expression of molecular effectors of cell migration on neural stem cells

To analyze expression of molecular effectors of Steps 1, 2 and 3/4 of cell migration, flow cytometry was performed on primary cultures of mouse NSCs. NSCs were devoid of reactivity with E-selectin-Ig chimera (E-Ig) and P-selectin-Ig chimera (P-Ig), indicating the absence of E- and P-selectin ligands (Figure 1A) even in the presence of inflammatory mediators (Supplementary data, Figure S1); they also did not stain with mAb CSLEX1, KM93 or HECA452 (each of which identify sLe^x). NSCs expressed CD44 and the integrins VLA-4 (CD49d/CD29) and VLA-5 (CD49e/CD29), as well as the chemokine receptor CXCR4; this pattern of NSC marker expression has been observed by others (Pluchino et al. 2003, 2005; Campos et al. 2004, 2006; Imitola, Raddassi, et al. 2004; Ji et al. 2004; Back et al. 2005; Leone et al. 2005) (Figure 1B). The NSCs also characteristically expressed NCAM in addition to the well-described polysialic acid (PSA) (Vitry et al. 2001) (Figure 1B). NSCs did not express PSGL-1, CD43, LFA-1 [lacking both CD11a (α_1) and CD18 (β_2) chains] and LPAM-1 ($\alpha_4\beta_7$) (Figure 1B). These results indicate that NSCs are defi-

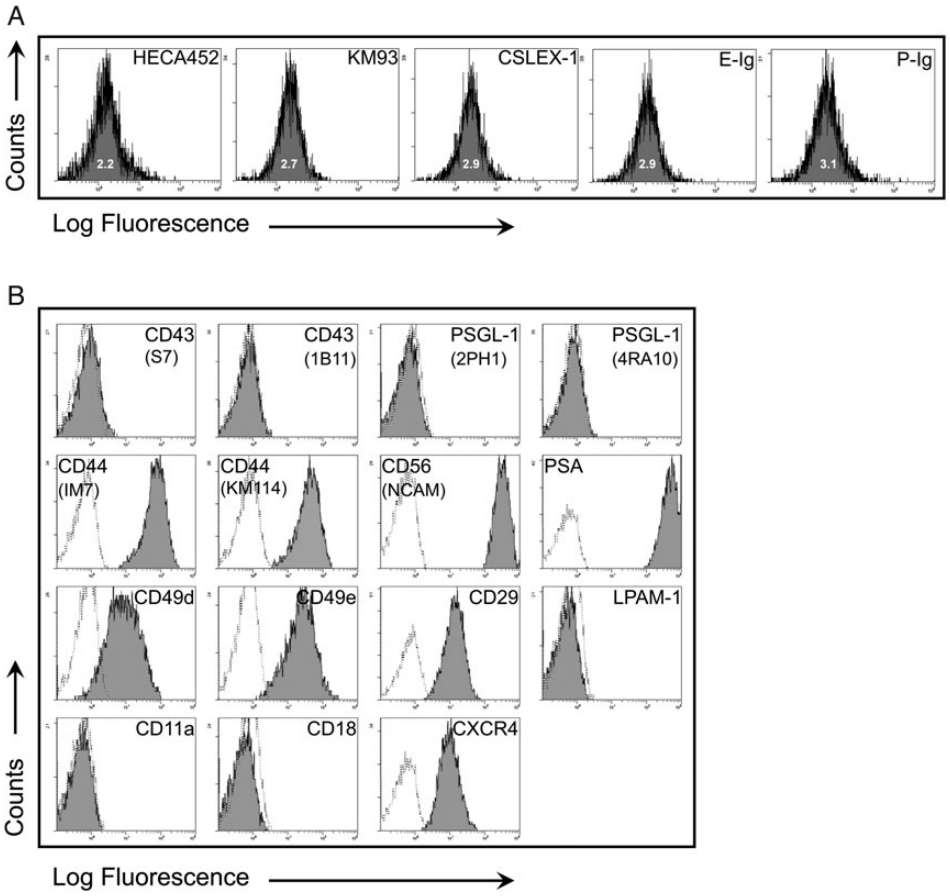

Fig. 1. NSCs lack E-selectin ligands but express a number of other cell surface adhesion molecules. (**A**) Flow cytometric analysis of HECA452, KM93, CSLEX-1, E-selectin ligand (E-Ig binding) and P-selectin ligand (P-Ig binding) expression on NSCs. The corresponding isotype controls showed overlapping signals for each antibody surveyed, i.e., rat IgM (for HECA-452; MFI: 1.9), mouse IgM (for KM93 and CSLEX-1; MFI: 2.7) and human IgG_1 (for E-Ig and P-Ig; MFI: 3.5). A histogram plot representing a typical E-Ig binding profile illustrates that over 99% of the cells consistently express E-Ig binding following GPS. (**B**) Flow cytometric analysis of CD43 (S7 and 1B11), PSGL-1 (2PH1, 4RA10), CD44 (IM7, KM114), NCAM (CD56), PSA, CD49d, CD49e, CD29, LPAM-1, CD11a, CD18 and CXCR4. The dotted line is isotype control, and the black line is specific antibody. All results displayed are representative of $n = 5$ flow cytometry experiments performed on NSCs.

cient in expression of Step 1 effectors of the multistep cascade of cell transmigration, yet express chemokine receptors and relevant integrin effectors that mediate Steps 2–4 in extravasation and that are also involved in their mobilization in the developing brain via radial migration (Imitola, Comabella, et al. 2004).

GPS enforces E-selectin ligand activity on neural stem cells

CD44, a molecule involved in migration of NSCs (Deboux et al. 2013) and brain cancer stem cells (Fu et al. 2013), is strongly expressed among NSCs in culture (Figure 1B). However, the finding that NSC lacks E-selectin binding (Figure 1A) indicates that these cells do not natively express the E-selectin-binding glycoform of CD44 known as HCELL (Dimitroff et al. 2000, 2001; Sackstein 2004). We thus sought to determine whether a nongenetic manipulation using GPS of CD44 glycans would enforce HCELL expression (Sackstein et al. 2008). To this end, we treated NSCs with the α(1,3)-linkage-specific fucosyltransferase, fucosyltransferase VI (FTVI). This enzyme specifically places a fucose onto a terminal type 2-lactosamine unit; if that lactosamine is capped with an α(2,3)-linked sialic acid, sLe^x is created. Following FTVI treatment of NSCs (GPS-NSC), reactivity with mAbs CSLEX1, KM93 and HECA452 was induced, consistent with strong expression of sLe^x epitopes (Figure 2A), with associated E-Ig binding (Figure 2A) but without induction of P-Ig binding (Figure 2A). Notably, expression of CD15 (also known as SSEA-1 or Le^x) is high in NSCs (Figure 2A), and although FTVI can fucosylate unsialylated terminal lactosamines thereby yielding CD15 (SSEA-1), the expression of CD15 was unchanged following enforced fucosylation (Figure 2A). As determined by microarray analysis of murine NSCs, the fucosyltransferases involved in creating these Le^x (CD15) structures on NSCs may be attributed to FTIX, FTX and FTXI (Supplementary data, Figure S2). Recent studies have implicated that FTX is involved in α-1,3-fucosyltransferase activity with strict substrate specificity (adding fucose to GlcNAc at the innermost core position of *N*-glycans and/or on bisecting *N*-glycans of glycoproteins) (Mollicone et al. 2009; Kumar et al. 2013) synthesizing Le^x only on restricted glycoprotein substrates that may not be common to the sialylated lactosamine structures recognized by other fucosyltransferases such as the FTVI. Altogether, these data indicate that α(1,3)-exofucosylation only occurred on sialylated lactosaminyl glycans. Bromelain digestion of NSCs prior to GPS treatment markedly reduced HECA452 reactivity

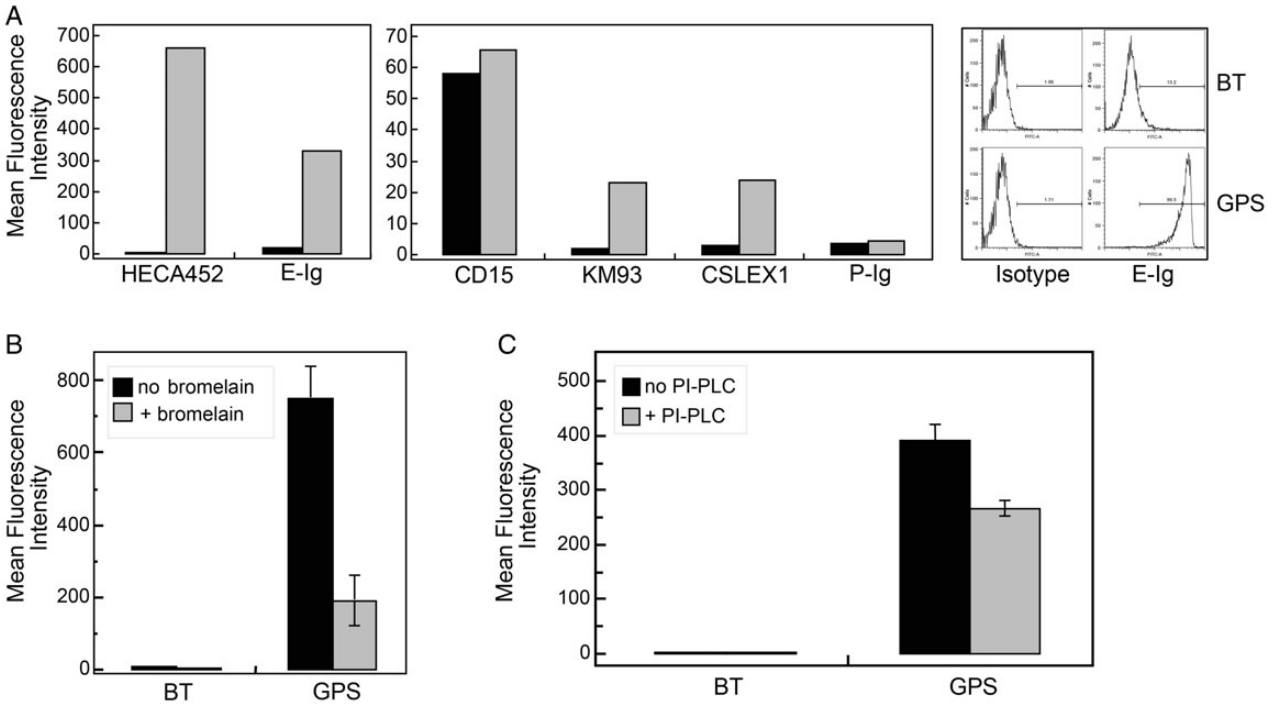

Fig. 2. GPS treatment of NSCs generates sialofucosylations mainly on glycoproteins, some of which are GPI-linked. (**A**) Flow cytometric analysis of HECA452, CD15, KM93, CSLEX1, E-Ig and P-Ig reactivity on BT-NSCs (control NSCs; black bars) and GPS-NSCs (FTVI-treated NSCs; gray bars). The corresponding isotype controls for each antibody surveyed were rat IgM (for HECA-452; MFI: 1.8), mouse IgM (for CD15, KM93 and CSLEX-1; MFI: 1.9) and human IgG_1 (for E-Ig and P-Ig; MFI: 3.2). Results displayed are representative of five separate experiments. (**B**) Flow cytometric analysis of HECA452 reactivity of GPS-NSCs undigested (black bars) or digested with bromelain (gray bars) prior to GPS treatment. Values are means ± SEM. ($n = 3$ for each group). (**C**) Flow cytometric analysis of HECA452 reactivity of GPS-NSCs undigested (black bars) or digested with PI-PLC (gray bars). Values are means ± SEM ($n = 3$ for each group).

(Figure 2B), demonstrating that glycoproteins, not glycolipids, were the predominant carriers of sialofucosylated determinants. Treatment of GPS-NSCs with phosphatidylinositol phospholipase C (PI-PLC) resulted in a modest but significant decrease in the HECA452 signal by flow cytometric analysis (Figure 2C), indicating that a minor population of sLe^x-decorated glycoproteins are glycophosphatidyl inositol (GPI)-linked.

Western blot of cell lysates and of immunoprecipitated CD44 from GPS-NSCs revealed that one of the glycoproteins decorated with the essential sialofucosylations recognized by HECA452 was the standard, unspliced form of CD44 (~100 kDa; Figure 3A), and CD44 also reacted with E-Ig (Figure 3A). However, following immunoprecipitation of CD44, other candidate glycoprotein E-selectin ligand(s) were identified by evidence of reactivity with E-Ig and HECA452 in the residual supernatant (SN) fraction. Two bands were apparent at ~120 and ~140 kDa. Based on the molecular weight profile of these bands (Figure 3A) and the partial PI-PLC sensitivity of E-selectin binding (Figure 2C), a characteristic of the 120 kDa form of NCAM (Gascon et al. 2007; Maness and Schachner 2007; Rutishauser 2008), we speculated that NCAM could be serving as an additional E-selectin ligand. We thus performed immunoprecipitation with a pan-NCAM mAb and observed that the residual bands persisting after immunoprecipitation of CD44 were indeed those of NCAM (Figure 3B). In addition, following immunoprecipitation of CD44 and exhaustive immunoprecipitation of NCAM, only a very anemic E-selectin signal was observed indicating that CD44 and NCAM were the major E-selectin ligands present after GPS treatment of NSCs (Supplementary data, Figure S3). To determine if the relevant sialofucosylations on NCAM were displayed on *N*-glycans, we tested E-Ig reactivity on western blot of lysates of GPS-NSCs following digestion with *N*-glycosidase F (PNGaseF) (Figure 3B); no evident staining with E-Ig following digestion was observed, indicating that the relevant E-selectin binding determinant(s) are displayed on *N*-glycans. The contribution of the GPI-anchored form of NCAM-E to overall sLe^x expression after enforced fucosylation of NSC is modest, as shown by a small decrease in HECA452 signal (and E-Ig signal—data not shown) following PI-PLC treatment (Figure 2C). Therefore, enforced α(1,3)-fucosylation of murine NSCs created HCELL as well as a unique E-selectin ligand reactive form of the neural precursor molecule NCAM, which we named "NCAM-E". Interestingly, human NSCs (CC-2599) only express HCELL and not NCAM-E following GPS treatment (Supplementary data, Figure S4).

To assess the stability of GPS-engineered E-selectin ligand activity on NSCs, we measured E-Ig reactivity by flow cytometry at 24 h intervals following enforced exofucosylation. E-selectin ligand activity was stable for up to 24 h, subsequently declining to undetectable levels by 72 h, presumably due to turnover of surface protein (Figure 3C). NSC viability (Supplementary data, Figure S5) was unaffected by enforced exofucosylation, and there were no differences in the number or proliferation of neurospheres in clonogenic assays or in differentiation of NSCs (Supplementary data, Figure S6). Thus, there were no evident phenotypic differences induced by GPS treatment of NSCs, except for creation of E-selectin ligands.

NSCs have been shown to inhibit the proliferation T cells in vitro (Einstein et al. 2006, 2007; Martino and Pluchino 2006), and, in

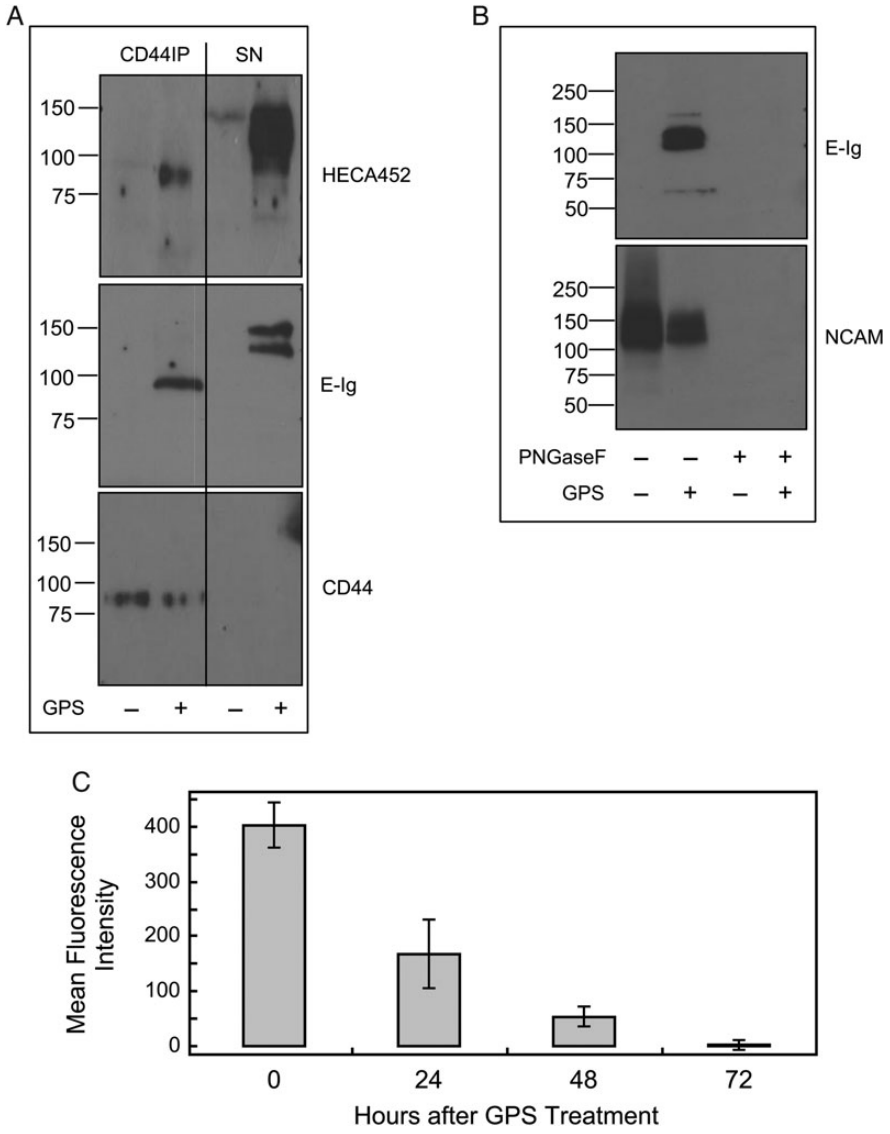

Fig. 3. GPS treatment of NSCs creates transient E-selectin ligands at 100, 120 and 140 kDa, which correspond to HCELL and NCAM-E. (**A**) CD44 was immunoprecipitated (with IM7 and KM114 mAb to CD44) from equivalent amounts of cell lysates from GPS-treated (+) or buffer-treated (–) NSCs. Western blot analysis was performed on immunoprecipitates of NSCs and SNs from the immunoprecipitates, which were electrophoresed and blotted with HECA452, E-Ig and CD44. (**B**) NCAM was next immunoprecipitated (with NCAM 13 mAb) from equivalent amounts of cell lysate SNs (that had underwent immunoprecipitation with CD44 mAbs as in A) from GPS-treated (+) or buffer-treated (–) NSCs lysates that had been either treated with PNGaseF (+) or not (–). Immunoprecipitates were then electrophoresed and blotted with E-Ig and NCAM. Staining with E-Ig was performed in the presence of Ca^{2+}. (**C**) NSCs were treated with GPS on Day 0 and cultured for another 3 days in normal growth media. Every 24 h, aliquots of cells were removed and assayed for E-selectin ligand activity by flow cytometry. See also Supplementary data, Figures S3 and S5–S7.

particular, to dampen mitogenic responses of T cells in vitro. To assess whether this immunoregulatory function of NSCs is affected by enforced E-selectin ligand activity, we examined the ability of GPS-NSCs and control buffer-treated NSCs (BT-NSCs) to suppress the proliferation of lymph node cells in response to Con A activation. As displayed in Supplementary data, Figure S7, both GPS- and BT-NSCs were able to decrease T cell proliferation as well as suppress the level of inflammatory cytokine production equally, suggesting that there is no immunomodulatory advantage or disadvantage provided by the GPS treatment itself on NSCs. Interestingly, we also observed equal release of leukemia inhibitory factor (LIF) from NSCs upon inflammatory cytokine treatment for both BT- and GPS-NSCs that was enhanced upon binding of GPS-treated cells to E-Ig (Supplementary data, Figure S7C). Thus, enforced exofucosylation of NSCs induced transient E-selectin ligand activity without undesirable effects on NSC phenotype or function as determined by in vitro studies.

GPS-NSCs display robust physiological rolling interactions with E-selectin

To analyze the potency of E-selectin ligand activity of GPS-NSCs under physiologic blood flow conditions, parallel plate flow chamber studies were performed using human umbilical vein endothelial cells (HUVECs) stimulated by cytokines (IL-1β and TNF-α) to express E-selectin. As shown in Figure 4A, GPS-NSCs exhibited prominent E-selectin ligand activity that was completely abrogated in the

presence of ethylenediaminetetraacetic acid (EDTA) or by the use of a blocking anti-E-selectin mAb. Significant shear-resistant rolling interactions were observed within usual post-capillary venular shear levels (1–4 dynes/cm^2) and persisted over 20 dynes/cm^2 (Figure 4A). To analyze which of the glycan-engineered E-selectin ligands, HCELL or NCAM-E, is the more potent E-selectin ligand on NSCs, we used the blot-rolling assay (Fuhlbrigge et al. 2002). This technique permits the detection of shear-dependent selectin ligand interactions on membrane proteins resolved by sodium dodecyl sulfate-polyacrylamide gel electrophoresis (SDS-PAGE), thus allowing the evaluation of the individual contribution of HCELL and NCAM-E to the E-selectin ligand activity of GPS-NSC. Accordingly, to evaluate the respective E-selectin binding properties, E-selectin-transfected CHO cells (CHO-E) were perfused over HECA-452-immunostained blots of GPS-NSC lysates.

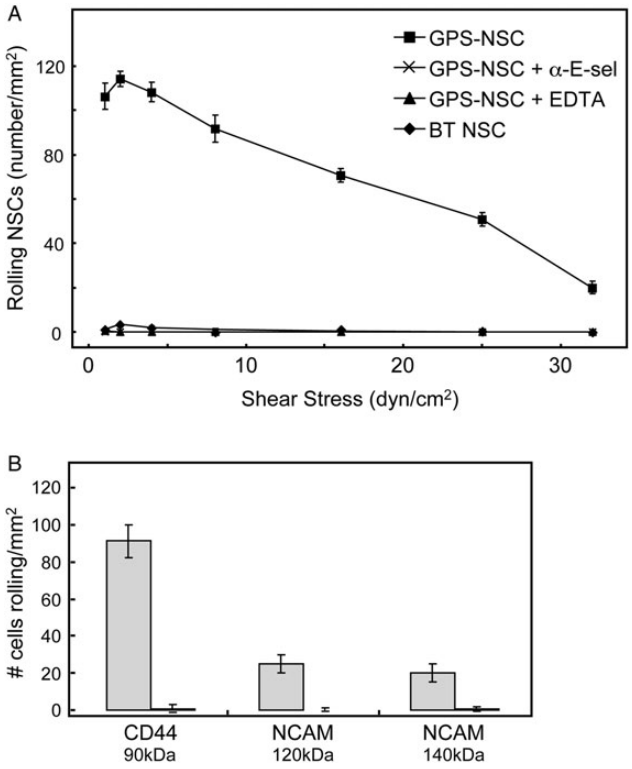

Fig. 4. GPS-NSCs have markedly enhanced shear-resistant adhesive interactions with endothelial E-selectin under defined shear stress conditions. (**A**) BT-NSCs or GPS-NSCs were perfused over IL-1β- and TNF-α-stimulated HUVEC at 1.0 dyne/cm^2. NSC accumulation was then determined at shear stresses of 1, 2, 4, 8, 16, 25 and 32 dynes/cm^2. GPS-NSCs show rolling adhesive interactions on HUVEC at a shear stress of up to 32 dynes/cm^2. To control for the specificity of binding of GPS-NSCs, EDTA was added to the assay buffer (EDTA group), or stimulated HUVECs were pretreated with a function-blocking mAb to E-selectin (anti-E-Sel group) before use in adhesion assays. Values are means ± SEM ($n = 4$ for each group). $P \leq 0.001$ for comparisons of GPS-NSCs with all other groups at all shear stress levels. (**B**) Adhesion bar graph for blot-rolling assay (rolling cells/mm^2) for CHO-E cells perfused over SDS-PAGE immunoblots of HECA-452-reactive membrane glycoproteins of NSCs at 0.6 dyne/cm^2. Immunoprecipitates of CD44/HCELL and pan-NCAM from both BT-NSCs (black bars) and GPS-NSCs (gray bars) were resolved by SDS-PAGE and blotted for HECA-452 prior to performing the assay. To control for the specificity of CHO-E binding to membrane glycoproteins, EDTA was added to the buffer containing the CHO-E cells before use in adhesion assays; no cells bound under this condition (data not shown). Results presented are representative of multiple runs ($n = 4$) on HECA-452 blots of multiple ($n = 3$) membrane preparations of NSCs.

As illustrated in Figure 4B, more CHO-E cells interacted and adhered to HCELL compared with either the 120 kD or the 140 kD forms of NCAM-E. CHO-E cells suspended in flow medium containing 5 mM EDTA had negligible adhesion to any regions of the blot, confirming Ca^{2+}-dependent binding consistent with selectin ligand activity.

GPS-NSCs exhibit increased homing and tissue infiltration in vivo in EAE

To assess whether injected NSCs infiltrated the CNS parenchyma, we performed confocal microscopy studies. To this end, GPS-NSCs and BT-NSCs were labeled with PKH26 dye and were injected intravenously (i.v.) into myelin oligodendrocyte glycoprotein (MOG)-induced chronic EAE mice in two separate i.v. injections: before disease onset [Day 9 post-immunization (PI)] and at the onset of the disease (Day 13 PI). These days were chosen based on prior studies of E-selectin expression on brain endothelium in EAE (Piccio et al. 2002). Lumbar-sacral spinal cords and brains were harvested 4 days (Day 17 PI) after the second NSC injection. Confocal analysis of the brain demonstrated both higher amounts of GPS-NSCs (Figure 5A) and localization outside of Flk-1$^+$ vessels in the brain (Supplementary data, Figure S8). Further, parallel analysis of the spinal cord (Figure 5B–D), where the majority of pathology occurs in EAE, demonstrated 2-fold greater numbers of extravascular GPS-NSCs infiltrates over BT-NSCs infiltrates by Day 17 PI (Figure 5D). These data indicate that GPS-NSCs infiltrate the CNS parenchyma significantly more effectively than BT-NSCs in both the brain and the spinal cord. To further confirm our confocal data, we studied the effect of GPS-engineered E-selectin ligand activity on short-term homing of NSCs in vivo. Syngeneic NSCs were stained using a fluorochrome tracking dye, carboxyfluorescein diacetate succinimidyl ester (CFDA-SE), and adoptively transferred into C57BL/6 mice on Days 9 and 13 PI with MOG as described in the *Materials and methods* section. Within 16 h after the second cell injection, we observed that GPS-NSCs accumulated in the brain, spleen and liver 3- to 5-fold more efficiently than BT-NSCs (Figure 5E). The relative advantage of GPS-NSCs in infiltrating the brain, spleen and liver reflected a true difference in trafficking and not simply the preferential expansion of these cells in situ, as their average CFDA-SE fluorescence was not reduced relative to BT-NSCs (data not shown). Indeed of those cells that migrated to the spleen, it is evident that there are close interactions of NSCs with CD4$^+$ T cells (Figure 5F). Injected cells also accumulated in the lungs, but without difference between GPS- and BT-NSCs, likely a reflection of steric trapping in pulmonary microvessels (Figure 5E). Thus, the sLe^x structure formed on NSCs following GPS treatment licenses migration of these cells into these organs and highlights the critical role of the E-selectin ligand activity in driving tissue-specific migration of NSCs in vivo.

GPS-NSCs increased homing translates into amelioration of neuropathology by enhanced endogenous indirect neuroregeneration in EAE

To address whether improved tissue homing of NSC had an enhanced therapeutic effect, we monitored the neurologic status of C57BL/6 mice receiving NSC injections following MOG-induced chronic EAE and analyzed clinical parameters as well as tissue repair and pathology. Neural precursors were administered in two separate i.v. injections on Days 9 and 13 PI. Five groups of EAE mice were tested: (1) GPS-NSCs, (2) BT-NSCs, (3) hank's balanced salt solution (HBSS) (sham; i.e., no cells), (4) BT-HSPC and (5) GPS-HSPC. The clinical score was evaluated daily in individual mice in a blind fashion

(Figure 6A), and the linear regression of cumulative burden of disease was calculated (Figure 6B and Table I). The injection of control NSCs (BT-NSC) attenuated the clinical severity of EAE compared with HSPC- and sham-treated animals ($P = 0.006$). However, i.v. injection of GPS-NSCs ($n = 30$) showed a more significantly improved clinical score compared with BT-NSCs ($n = 30$; $P = 0.006$), GPS-HSPC ($n = 30$; $P < 0.0001$), BT-HSPC ($n = 30$; $P < 0.0001$) and sham ($n = 30$; $P < 0.0001$) treated animals. It is important to note that this amelioration of disease severity is specific to NSCs, since neither the injection of GPS-HSPC [which display markedly increased E-selectin ligand activity, see Supplementary data, Figure S9A (Merzaban et al. 2011)] or the injection of BT-HSPC showed an improvement in the clinical score of MOG-induced animals compared with control animals (Supplementary data, Figure S9B, C and Table S1). Indeed, injection of either GPS- or BT-HSPCs showed a trend toward worsened clinical outcomes indicating that the observed salutary effects of NSC infusion are not a general property of adult stem cells.

Notably, examination of the neuropathology at Day 30 after EAE induction showed statistically significant differences in several parameters of inflammation and neuroregeneration in mice that received GPS-NSC compared with BT-NSC- and sham-treated animals (Figure 6C). To determine the impact of NSC injections on the neuropathology of EAE, we evaluated a number of different markers. First, to assess the extent of inflammation, we stained sections of spinal cord from each study group of mice for CD11b, a marker that identifies infiltrating macrophages and microglia. Animals with EAE that received HBSS buffer alone displayed high levels of staining for CD11b, with cells exhibiting increased numbers of membrane processes, morphologic evidence of an activated phenotype (Figure 6C). The numbers of CD11b-stained cells were significantly decreased in mice that received BT-NSCs ($P < 0.0001$), and notably, these levels were even further decreased in animals injected with GPS-NSCs ($P < 0.005$ compared with BT-NSCs). Importantly, the macrophage/microglia displayed decreased CD11b staining and more discrete membrane processes indicative of decreased activation (Figure 6C). In addition, quantification of brain $CD4^+$ T cells in the different treatment groups revealed a significant decrease of infiltrating T cells in animals given GPS-NSCs (Figure 6D and E). To assess neuroregeneration, we stained sections of spinal cord for the markers GAP-43 and SMI-32 (Figure 6F–I). In animals injected with GPS-NSCs, there was increased expression of GAP-43, a molecule associated with axon integrity and regeneration, compared with that in mice that received either BT-NSCs or HBSS buffer alone (Figure 6F–G). Conversely, a specific reduction in the expression of SMI-32, a marker of axonal degeneration, was observed in animals that received GPS-NSCs compared with mice receiving either BT-NSCs or HBSS buffer (Figure 6H and I). These data support the notion that the improved clinical effects afforded by GPS-NSCs over BT-NSCs are secondary to increased lesional migration of tissue-specific NSC yielding enhanced neuroprotection.

To further assess whether observed effects of GPS-NSCs reflect increased neuroregeneration, we stained for markers associated with oligodendrogenesis and mature oligodendrocytes, including CNPase, Olig-2 and SOX9. We observed a statistically significant enhancement in the number of Olig-2, SOX9 and CNPase cells in animals that received GPS-NSCs compared with BT-NSCs or sham control (Figure 6D and E). Although there was evidence of injected NSCs at Day 17 PI ($SOX\text{-}2^+$ cells; Supplementary data, Figure S8), we did not observe persistent colonization by NSC (tagged with GFP) at 30 days PI (Supplementary data, Figure S10) in any of the injection groups, suggesting that the mechanism of NSC neuroprotection associated with improved homing does not necessitate the continued presence nor differentiation toward neural lineage cells, of administered NSCs. Altogether, these data indicate that the treatment of mice with GPS-NSCs enhanced the delivery of NSCs to the CNS, resulting in improved endogenous tissue regeneration.

Discussion

EAE is a model of a chronic, demyelinating disease of the CNS characterized by multifocal inflammatory lesions yielding gradual destruction of the myelin sheath, leading to axonal injury and loss (Imitola et al. 2006). Stem cell-based therapeutics offers the promise of repair of damaged/inflamed tissue by replacing affected cells (direct regeneration) and/or by production of supportive/trophic factors in the milieu that evoke tissue regeneration by endogenous cells (indirect regeneration). In the case of disseminated neurologic diseases like MS, use of tissue-specific NSCs could prove clinically useful in achieving CNS recovery, but a proximate hurdle to accomplishing this goal is to deliver adequate numbers of cells to the sites of neural injury. Prior studies have shown a benefit of transplanted NSCs in experimental models of stroke, spinal cord trauma and MS (Ben-Hur et al. 2003; Pluchino et al. 2003, 2005; Imitola, Raddassi, et al. 2004; Einstein et al. 2006, 2007; Ziv et al. 2006; Lee et al. 2008). Direct injection into the affected site was used as route of delivery in these studies; however, in order to attain appropriate colonization of NSC within affected tissue(s) in multifocal CNS diseases, the vascular route of delivery is required as local administration (i.e., in situ injection) is impractical given the diffuse nature of disease and associated anatomic constraints. To date, there have been no studies to evaluate the expression of molecular effectors of cell migration on NSCs, and, more importantly, no studies to address how optimizing expression of such effectors could enhance NSC neurotropism.

Our studies reveal that NSCs express relevant Step 2–4 effectors, but are conspicuously deficient in Step 1 effectors: (1) they do not natively express ligands for E-selectin or P-selectin [even when grown in the presence of inflammatory cytokines (Supplementary data, Figure S1)]; (2) they lack expression of the glycan sLe^x, which is the canonical selectin binding determinant and (3) they do not express the glycoprotein PSGL-1, a selectin ligand on myelin-specific Th1 cells that has been reported to mediate trafficking to the brain (Piccio et al. 2002, 2005). Importantly, expression of endothelial selectins, especially E-selectin, has been implicated in recruitment of immunologic effectors in MS and EAE (Lee and Benveniste 1999; Piccio et al. 2002). Thus, we sought here to assess whether glycan engineering of NSC to enforce expression of E-selectin ligands would enhance systemic delivery of the cells and, in consequence, have biologic effects in EAE.

The dataset here shows that cultured NSCs express two well-characterized neural cell surface molecules, CD44 and NCAM (Pluchino et al. 2003; Back et al. 2005). Strikingly, exofucosylation of mouse NSCs yielded high expression of sLe^x determinants prominently on these glycoproteins, programming conversion of CD44 into the potent E-selectin ligand HCELL (Dimitroff et al. 2000, 2001) and also inducing expression of two sialofucosylated glycoforms of NCAM of ~120 and ~140 kDa, which we designate "NCAM-E". Blot-rolling assays revealed that HCELL is the principal E-selectin ligand expressed on GPS-NSCs (Figure 4B). These findings are corroborated by results of flow cytometry following the removal of NCAM-E by PI-PLC digestion, showing considerable retention of NSC sLe^x expression and E-Ig reactivity (Figure 2C).

NCAM, a member of the immunoglobulin superfamily, is expressed on both neurons and glia and is conventionally viewed as a

mediator of cell–cell interactions establishing a physical anchorage of cells to their environment. Posttranslational glycan modifications consisting of α-2,8-linked PSA on the NCAM protein core provide unique properties in neural migration (Gascon et al. 2007; Maness and Schachner 2007; Rutishauser 2008), and PSA-NCAM appears to play a crucial role in mediating precursor cell migration in the brain (Zhang et al. 2004; Lavdas et al. 2006; Glaser et al. 2007). Our data now provide the first evidence that NCAM displays relevant terminal α-(2,3)-sialyllactosaminyl glycans that can serve as acceptors for exofucosylation to create sLe^x determinants. Following cell surface glycoengineering of NSCs, PSA expression levels did not change and the induced E-selectin ligand activity is not permanent, as there was complete loss of sLe^x expression within 72 h of enforced fucosylation (Figure 3). Thus, subsequent to extravasation, temporal reversion to native NCAM should occur, and infiltrating NSCs would then be capable of undergoing endogenous NCAM-mediated intraparenchymal CNS migration. Notably, though murine NSCs express NCAM bearing α-(2,3)-sialyllactosaminyl glycans, our studies of human NSCs (CC-2599) indicate that these cells only express HCELL and not NCAM-E following exofucosylation (Supplementary data, Figure S4); thus, human NSC may express relevant sialolactosaminyl glycans that serve as acceptors for enforced fucosylation only on CD44. These species differences should be considered when interpreting xenograft studies where human NSCs are used in rodent systems (Goncharova et al. 2014).

The induction of E-selectin ligand activity has profound implications for cell trafficking, serving to direct cell migration to endothelial beds that express E-selectin. As shown by others, we observed that NSCs display the chemokine receptor CXCR4 and the integrin VLA-4 (see Figure 1). It has been shown that expression of CXCR4 on human NSCs (Flax et al. 1998; Bezzi et al. 2001; Imitola, Raddassi, et al. 2004) promotes migration in vivo toward CNS injury wherein local astrocytes and endothelium upregulate the cognate ligand stromal cell-derived factor 1α (SDF-1α, also known as CXCL12) (Imitola, Raddassi, et al. 2004). These observations define CXCR4 as a prominent Step 2 effector in promoting NSC homing to CNS injury. The corresponding endothelial receptor for VLA-4, VCAM-1, is also upregulated in the inflammatory response of the brain to injury (Justicia et al. 2006). The VLA-4/VCAM-1 axis has similarly been shown to play a critical role in migration of NSCs, in that only NSCs that constitutively express VLA-4, in addition to CXCR4, were able to accumulate around inflamed CNS microvessels in affected lesions in EAE (Pluchino et al. 2005). A recent xenograft study suggests that integrins may play a role as Step 1 mediators of migration on human NSCs in a rat stroke model suggesting that selectin interactions are not necessary in this model system (Goncharova et al. 2014). Although further work is warranted, the varying role(s) of integrins as mediators of Step 1 interactions could reflect differences in the inflammatory model used, the host animal system, the permeability of vessels, the expression of endothelial adhesion molecules at that site of inflammation, the presence of soluble adhesion molecules at the site and the physical properties of the vessel that dictate the flow rate (i.e., diameter of vessel) (Berlin et al. 1995; Ding et al. 1999; Zarbock et al. 2007, 2012). In any case, expression of E-selectin ligands as Step 1 effectors on NSCs would serve to complement the constitutive expression of CXCR4 and VLA-4, thereby optimizing the recruitment of NSCs to inflammatory sites. Accordingly, though we observed that intravenously administered (non-modified) BT-NSCs can infiltrate the brain of EAE mice (Figure 5E), enforced E-selectin ligand expression by glycoengineering (as determined by above in vitro assays) yielded markedly increased migration of NSCs to the brain. This increased neurotropism was associated with markedly diminished CNS inflammation (Figure 6). Moreover, as shown in Figure 5, NSC accumulation in the CNS parenchyma was 2-fold higher among GPS-NSCs than BT-NSCs by Day 17 PI, indicating that enforced expression of Step 1 effectors promotes extravasation.

In addition to enhanced neurotropism, short-term homing data also revealed a significantly higher accumulation of GPS-NSCs in the spleen and the liver than in BT-NSCs (Figure 5E). These findings are consistent with results of a study reporting that systemically administered NSCs tend to accumulate in the brains of mice with EAE, and also in the spleen and the liver (Politi et al. 2007). E-selectin expression in the spleen has been described in humans, non-human primates and rodents (Redl et al. 1991; Drake et al. 1993; Schweitzer et al. 1996; Alam et al. 2000), and is upregulated by pro-inflammatory cytokines that are characteristically expressed in CNS inflammatory conditions (Weishaupt et al. 2000; Emamgholipour et al. 2013); indeed, conjugation of sLe^x to polymers has been shown to markedly enhance the accumulation of such polymers within the spleen (Horie et al. 2000, 2004), providing direct evidence that sLe^x expression promotes splenic delivery. It has been reported that infiltration of the spleen by NSCs dampens production of inflammatory cytokines by resident spleen cells (e.g., macrophages) resulting in anti-inflammatory effects (Lee et al. 2008). Other studies have reported that intravascularly administered NSCs provide peripheral immunosuppression (Einstein et al. 2006, 2007) or local immunomodulation that restrains CNS injury, rather than by enhancing neuroregeneration (Martino and Pluchino 2006; Pluchino et al. 2009; Wang et al. 2009). Thus, the observed increased splenic homing by enforced expression of E-selectin ligand activity on NSCs could be contributory to neuroprotection via immunomodulation by virtue of increased tissue ratio of NSCs to immune cells. This notion is supported by our in vitro data showing that although GPS-NSCs did not confer an immunomodulatory advantage compared with that observed with control NSCs, as the ratio of input NSCs to splenocytes is increased, T cell proliferation decreases (Supplementary data, Figure S7A).

Previous studies of cell surface exoglycosylation had utilized human mesenchymal stem cells in a xenotransplant model and did not address the therapeutic impact on tissue injury, i.e., whether glycoengineered stem cells would home to a site of inflammation and whether such cells would have desired regenerative and/or tissue-protective effect(s). Though enhanced recruitment of NSCs to the CNS was observed following infusion of GPS-NSCs, there was no commensurate increase in long-term engraftment of NSCs. Thus, though enhanced CNS infiltration was achieved by exploiting physiologic cell migration (i.e., in a noninvasive fashion that would preserve CNS tissue microenvironmental architecture), we did not observe that administered NSCs differentiated into progeny that regenerate functional CNS tissue in situ (i.e., through direct regeneration). In fact, we observed that administration of GPS-NSCs improved the ability of endogenous neuronal progenitors to become oligodendroglia (Figure 6D and E) as suggested by the increase in CNPase staining, a marker of mature oligodendrocytes. In order to correlate with differentiation in vivo, we quantified the expression of Sox-9 and Olig-2, two independent transcription factors associated with oligodendrogenesis that are expressed in oligodendrocyte precursors. Taken together, our results suggest that NSC infiltrates support oligodendrogenesis. However, our findings do not provide evidence for NSC-based direct neuroregeneration but instead suggest that the predominant role of NSCs in CNS tissue repair is via trophic effects that prime repair by endogenous cells (Phinney and Prockop 2007; Hess and Borlongan 2008; Caplan 2009; Laterza et al. 2013). Consistent

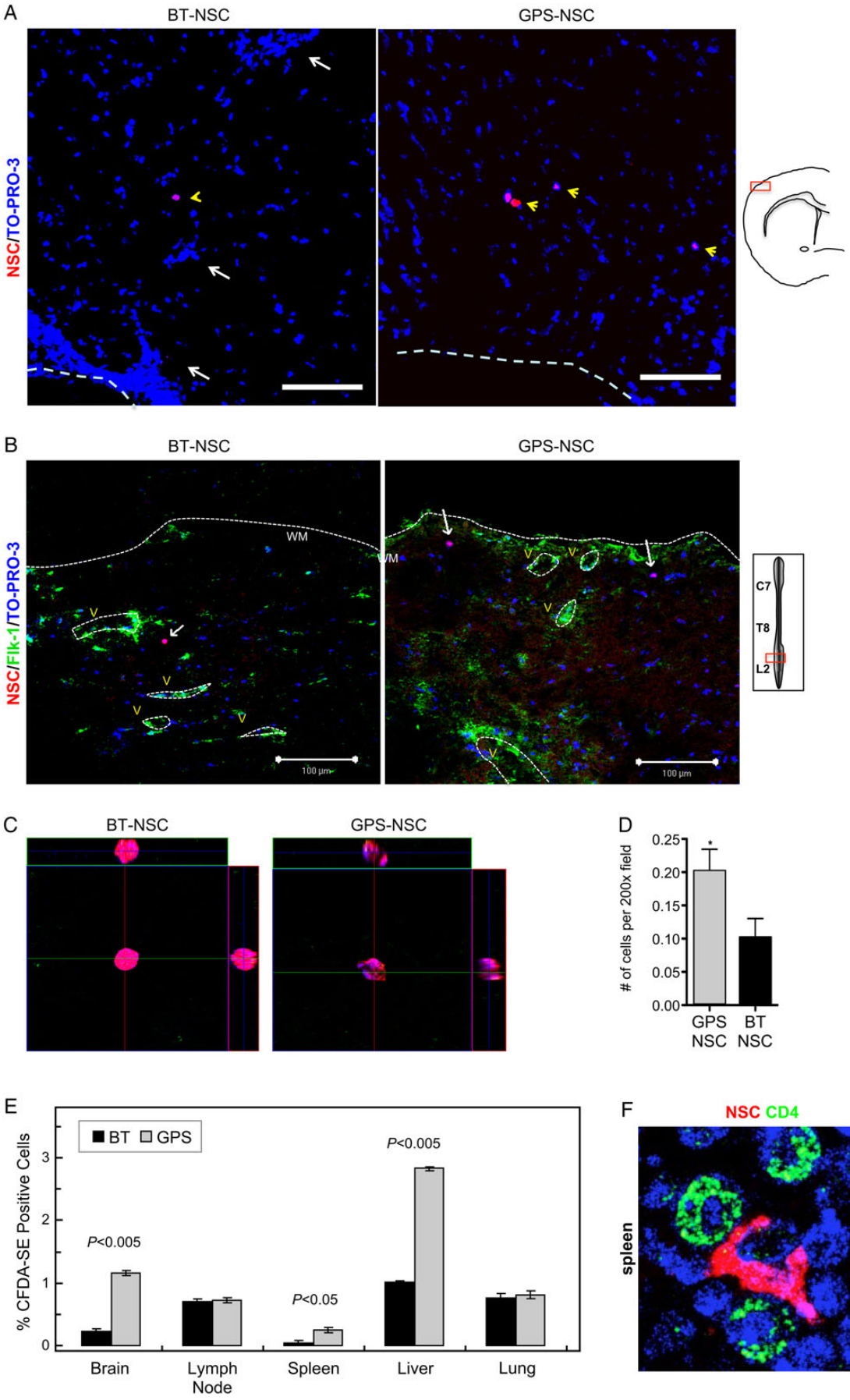
A
BT-NSC
GPS-NSC
NSC/TO-PRO-3
B
BT-NSC
GPS-NSC
NSC/Flk-1/TO-PRO-3
WM
V
100 µm
C7
T8
L2
C
BT-NSC
GPS-NSC
D
# of cells per 200x field
0.25
0.20
0.15
0.10
0.05
0.00
*
GPS NSC
BT NSC
E
% CFDA-SE Positive Cells
BT GPS
P<0.005
P<0.005
P<0.05
Brain
Lymph Node
Spleen
Liver
Lung
F
NSC CD4
spleen

with this notion, undifferentiated NSCs have been reported to significantly reduce scar formation and increase survival and function of endogenous glial and neuronal progenitors through the secretion of neurotrophins such as LIF (Laterza et al. 2013). In addition, NSCs support the formation of injury-induced growth niches through the expression of molecules such as BMP-4 and Noggin (Imitola, Raddassi, et al. 2004; Pluchino et al. 2005) that trigger indirect neuroregeneration by endogenous cells.

Collectively, our data support a mechanism in which glycan engineering of NSC to enforce expression of E-selectin ligands heightens tissue colonization, mediating immunomodulation and tissue repair without necessitating persistent/long-term engraftment of administered NSCs. Notably, despite enhanced E-selectin ligand activity, infusion of GPS-HSPC did not improve the course of EAE (indeed, injection of HSPC worsens disease, see Supplementary data, Figure S9 and Table S1), indicating that the observed neuroprotective effects of GPS-NSCs are not a general property of adult stem cells and are due to intrinsic factors related to NSCs. Consistent with this finding of adult stem cell-specific biologic effect(s), human HSPCs have been found to elicit strong host immune rejection in a mouse model of congenital corneal disease, while other adult stem cells such as mesenchymal stem cells suppress the host immune response (Liu et al. 2010). Though further studies on the molecular mechanism(s) mediating the observed neuroprotection by NSCs are warranted, our results indicate that cell surface glycan engineering did not change the self-renewal capacity, differentiation potential or alter the innate immunomodulatory capacity of NSCs. Collectively, the data presented here lead us to propose a model (Supplementary data, Figure S11) whereby enforced E-selectin ligand expression via exofucosylation of the surface of NSCs yields increased tissue recruitment at CNS inflammatory sites, thereby enhancing payload delivery of NSC trophic factors where they are needed. Because E-selectin expression is markedly upregulated at endothelial beds at all sites of inflammation in humans, our findings have profound translational implications for future clinical trials exploiting cell surface glycan engineering to improve the efficacy of stem cell therapeutics for MS as well as other devastating multifocal inflammatory diseases.

Materials and methods

Ethics statement

All mouse experiments were performed in accordance with the National Institutes of Health guidelines for the care and use of animals and under approval of the Institutional Animal Care and Use Committees of Harvard Medical School. The following are the specifics related to using mice in these experiments. *Justification for use*: EAE is a valuable model for the human disease MS. There are no mathematical models, computer simulations or in vitro systems that can substitute for the in vivo disease. Many of the treatments available for MS and other autoimmune diseases were first tested and their mechanisms investigated in EAE. MOG-induced EAE in C57/BL6 mice is valuable because of the availability of many knockout and transgenic mice on that background. *Veterinary care*: Mice are handled and cared for according to federal, institutional and association for assessment and accreditation of laboratory animal care guidelines. *Procedures to minimize adverse effects*: After immunization, animals are examined daily. Those affected by EAE develop a floppy tail (Grade 1), partial hind limb paralysis (Grade 2), complete hind limb paralysis (Grade 3), quadriparesis (Grade 4), moribund or animal death (Grade 5). Most animals have a Grade 0–3, and, rarely, animals reach Grade 4, and in such cases, euthanasia is performed. When animals are affected by EAE, they are provided with gel packs to ensure access to fluids and are provided with access to food within the cage. Euthanasia is performed by CO_2 inhalation administered according to institutional guidelines.

Reagents

The following antibodies were purchased from BD Pharmingen (MA, USA): function-blocking mouse anti-human E-selectin (68-5H11; IgG1), rat anti-human cutaneous lymphocyte antigen (CLA) (HECA-452; IgM), mouse anti-human sLe^x (CSLEX-1; IgM), mouse anti-human CD15 (IgM), rat anti-mouse PSGL-1 (2PH1 and 4RA10; IgG1), mouse anti-human PSGL-1 (KPL-1; IgG1), rat anti-mouse CD44 (KM114 and IM7; IgG1), mouse anti-human CD44 (515; IgG1), rat anti-mouse CD43 (S7; IgG2a), mouse anti-human CD43 (1G10; IgG1), mouse anti-(mouse anti-adult and embryonic pan N-Cam) CD56 (NCAM13; IgG2b), mouse anti-human CD56 (NCAM16.2; IgG2b), rat anti-human CXCR4 (2B11; IgG2b), mouse anti-human CXCR4 (12G5; IgG2a), rat anti-mouse CD18 (GAME-46; IgG1), rat anti-mouse CD29 (KM16; IgG2a), rat anti-mouse CD49d (9C10; IgG2b), rat anti-mouse CD11a (2D7; IgG2a), rat anti-mouse CD11b (M1/70; IgG2b), rat anti-mouse CD49e (MFR5; IgG2a), mouse IgG1,κ isotype, mouse IgG2a isotype, mouse IgM isotype, rat IgG isotype, rat IgM isotype and human IgG_1 isotype. The following secondary antibodies were also purchased from BD Pharmingen (MA, USA): phycoerythrin (PE) Streptavidin, biotin anti-rat IgM and goat anti-mouse Ig-HRP. The following secondary antibodies were purchased from Southern Biotech. (AL,

Fig. 5. GPS-NSCs exhibit improved homing in an EAE model in vivo. (**A–D**) GPS-NSCs migrate to the CNS parenchyma more efficiently than BT-NSCs. About 1×10^6 GPS-NSCs or BT-NSCs were labeled with PKH26 dye and were injected intravenously to MOG-induced EAE mice on Days 9 and 13 PI. (A) Analysis of the forebrain of EAE mice (on Day 17 PI) that either received BT-NSCs or GPS-NSCs revealed that lower numbers of PKH26-positive cells are seen in animals injected with BT-NSCs compared with GPS-NSCs. The yellow arrowheads indicate NSCs, and the white arrows indicate infiltrates. The white dashed line indicates meningeal borders. Supplementary data, Figure S8, show further analysis of these sections to confirm that the NSCs (PKH26; red) are located outside of Flk-1 vessels (green) and that they are SOX-2 positive (green). (B) Lumbar-sacral spinal cords (insert) were harvested on Day 17 PI. At Day 17 PI, more GPS-NSCs migrated out of the blood vessels into the spinal cord parenchyma than BT-NSCs. Blood vessels were visualized by Flk-1 (VEGFR2; green) staining. The edge of the spinal cord parenchyma is highlighted with a white dotted line. NSCs labeled with PKH26 dye are shown in red, and nuclei counterstained with TO-PRO-3 are blue. WM, white matter; V, blood vessels. (C) The insets show a 3D view of the migrated NSCs indicated by the arrows in A. (D) Quantification of numbers of BT-NSCs and GPS-NSCs per 200× migrating per spinal cord area at Day 17 PI were determined. A significant increase in the numbers of migrating GPS-NSCs over BT-NSCs was evident, $^*P < 0.05$. (**E**) Quantification of biodistribution of NSCs. GPS-NSCs (gray bars) or BT-NSCs (black bars) were labeled with CFDA-SE and injected intravenously into syngeneic MOG-treated C57BL6 mice on Days 9 and 13 PI. The brain, lymph nodes, spleen, liver and lung were analyzed 16 h after the last injection to determine the percentage of CFDA-SE-positive cells present within a defined gate representing NSCs. Non-EAE mice that received GPS-NSCs or BT-NSCs were used to standardize the signals observed in each tissue tested. Mice that did not receive cells were used to determine the background signal. Error bars represent the standard error of the mean. Data are representative of two separate experiments where 10 mice per group were tested. (**F**) In vivo confocal demonstration that NSCs are found in close contact with CD4 T cells in the spleen in vivo (NSCs are labeled pink and CD4 T cells in green).

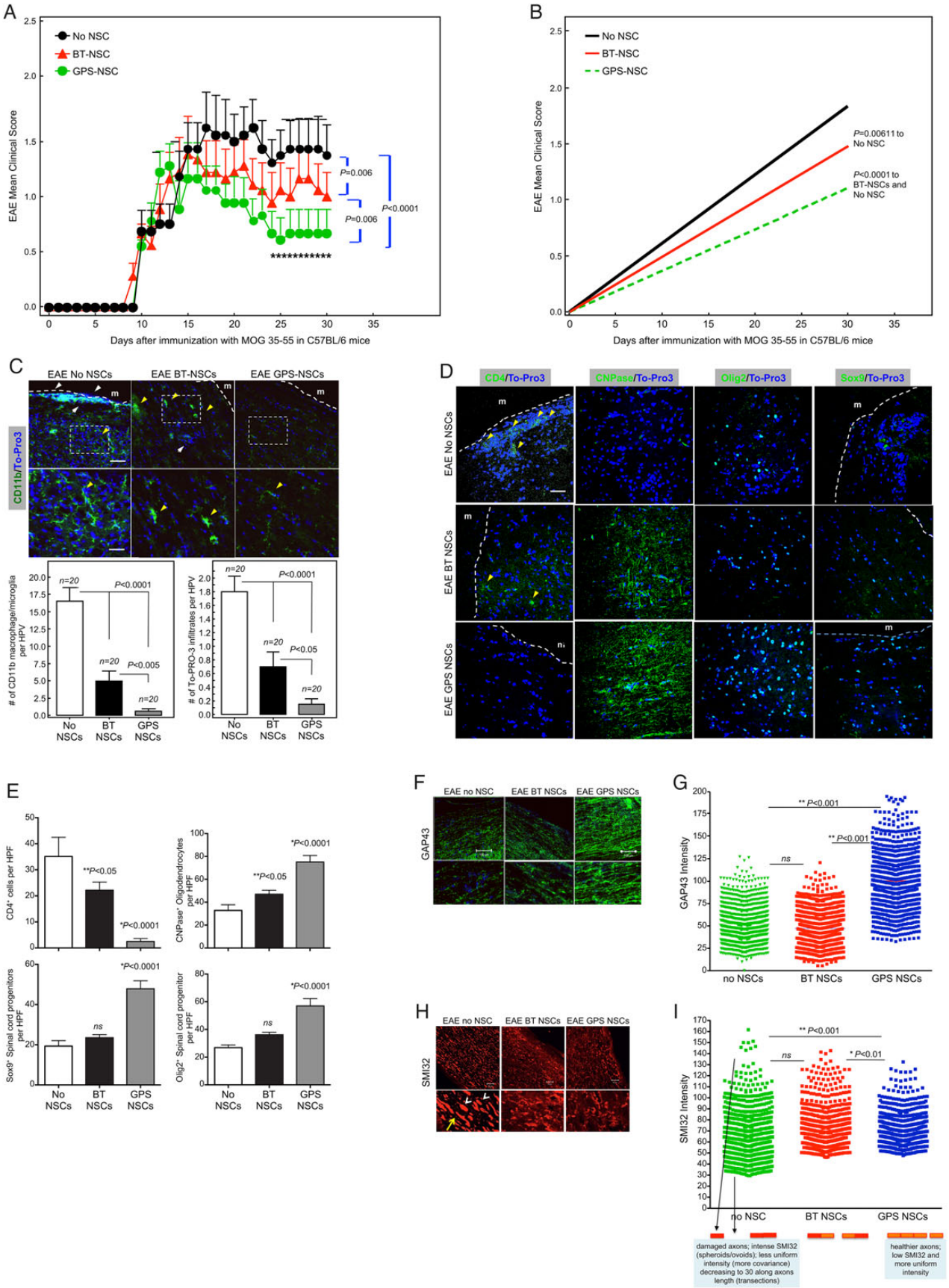
A
No NSC
BT-NSC
GPS-NSC
EAE Mean Clinical Score
Days after immunization with MOG 35-55 in C57BL/6 mice
P=0.006
P<0.0001
P=0.006
****
B
No NSC
BT-NSC
GPS-NSC
EAE Mean Clinical Score
Days after immunization with MOG 35-55 in C57BL/6 mice
P=0.00611 to No NSC
P<0.0001 to BT-NSCs and No NSC
C
EAE No NSCs
EAE BT-NSCs
EAE GPS-NSCs
CD11b/To-Pro3
# of CD11b macrophage/microglia per HPV
# of To-PRO-3 infiltrates per HPV
n=20
P<0.0001
P<0.005
P<0.05
No NSCs
BT NSCs
GPS NSCs
D
CD4/To-Pro3
CNPase/To-Pro3
Olig2/To-Pro3
Sox9/To-Pro3
EAE No NSCs
EAE BT NSCs
EAE GPS NSCs
E
CD4+ cells per HPF
CNPase+ Oligodendrocytes per HPF
Sox9+ Spinal cord progenitors per HPF
Olig2+ Spinal cord progenitor per HPF
**P<0.05
*P<0.0001
ns
No NSCs
BT NSCs
GPS NSCs
F
EAE no NSC
EAE BT NSCs
EAE GPS NSCs
GAP43
G
GAP43 Intensity
** P<0.001
ns
no NSCs
BT NSCs
GPS NSCs
H
EAE no NSC
EAE BT NSCs
EAE GPS NSCs
SMI32
I
SMI32 Intensity
** P<0.001
ns
* P<0.01
no NSC
BT NSCs
GPS NSCs
damaged axons; intense SMI32 (spheroids/ovoids); less uniform intensity (more covariance) decreasing to 30 along axons length (transections)
healthier axons; low SMI32 and more uniform intensity

Table I. EAE features in C57BL/6 mice treated intravenously with GPS-treated NSCs

Treatment	Route of cell administration	No. of mice	Disease onset (days PI)	Maximum clinical score	Cumulative disease score (0–20 PI)	Cumulative disease score (21–30 PI)
No NSC	–	30	13.22 ± 0.6	2.2 ± 0.4	15.75 ± 0.6	14.9 ± 2.4
NSCs BT	i.v.	30	12 ± 0.6	2.1 ± 0.3	12.3 ± 0.9	10.9 ± 2
NSCs-GPS	i.v.	30	12.2 ± 0.5	1.8 ± 0.1 *ns*	10.8 ± 1.4 *ns*	7.1 ± 1.5*

*$P < 0.05$ ANOVA multiple comparisons. PI; post immunization.

USA): rabbit anti-human IgG-biotin, goat anti-mouse IgM-PE, goat anti-rat IgG-PE, goat anti-mouse Ig-biotin, goat anti-rat Ig-HRP and goat anti-human Ig-HRP. Recombinant mouse E-selectin/human Ig chimera (E-Ig) and recombinant mouse P-selectin/human Ig chimera (P-Ig) were from R&D Systems (MN, USA). Mouse anti-human sLe^x (KM93; IgM) was purchased from Calbiochem (MA, USA). Rat anti-mouse CD43 (1B11; IgG2a) was purchased from Biolegend (CA, USA). Rat anti-mouse LPAM-1 (DATK32; IgG2a) and mouse anti-SMI32 (SMI-32; IgG1) were purchased from Abcam (MA, USA). Mouse anti-human CD15 (80H5; IgM) was purchased from Coulter-Immunotech (CO, USA). PNGase F was purchased from New England Biolabs (MA, USA). PI-PLC, bromelain, soybean trypsin inhibitor (SBTI), DNase and mouse anti-Map2 (HM-2; IgG1) were purchased from Sigma (MO, USA). Mouse anti-GFP (B2, IgG_{2a}) was purchased from Santa Cruz Biotechnology, Inc. (CA, USA). To-pro3 was purchased from Invitrogen (NY, USA). Mouse anti-human PSA (IgG2a) was a kind gift from Dr. Nicholas Stamatos. Fucosyltransferase VI (FTVI) enzyme was a gift of Dr. Roland Wohlgemuth (Sigma-Aldrich).

Cells

Mouse NSCs were isolated and cultured as described previously (Imitola, Comabella, et al. 2004; Imitola, Raddassi, et al. 2004). Briefly, a suspension of dissociated NSCs (5×10^5 cells per mL), isolated from the telencephalic VZ of embryonic day 12, was cultured in 98% Dulbecco's modified Eagle's medium (DMEM)/F12 (GIBCO), 1% N_2 supplement (GIBCO), 1% penicillin/streptomycin (GIBCO), 8 mg/mL heparin (Sigma), 10 ng/mL leukemia inhibitory factor (LIF, Chemicon), 20 ng/mL bFGF (Calbiochem) in uncoated 25 cm^2 flasks (Falcon) at 37°C in 5% CO_2. NSCs were used after second passage for most experiments. Single-cell suspension of NSCs was achieved by mechanical dissociation of the neurospheres in Versene (Life Technologies).

For isolation of mouse HSPC, bone marrow was harvested from the femur and tibia of C57BL/6 mice and single-cell suspensions were made. Red blood cells were lysed using red blood cell lysing buffer (Sigma; MO, USA). Cells were then washed and filtered through a 100 μm cell strainer (BD Falcon) prior to lineage depletion using the Lineage Cell Depletion Kit from Miltenyi Biotec (MA, USA). Cell preparations were depleted using the autoMACS™ Separator (Miltenyi Biotec.). Following depletion, the cells were then positively selected for c-kit using CD117 MicroBeads (Miltenyi Biotec.). The resulting $Lineage^{neg}C\text{-}kit^{pos}$ population (referred to as HSPC) was used for in vivo EAE mouse studies.

Chinese hamster ovary cells transfected with full-length E-selectin (CHO-E) and were maintained as described previously (Dimitroff et al. 2001). The human βFGF-dependent NSC cell line, CC-2599, was cultured as previously described (Imitola, Raddassi, et al. 2004) and used for data presented in Supplementary data, Figure S4.

Fig. 6. GPS-NSCs contribute to significant amelioration of EAE symptoms through enhanced neuroprotection. (**A**) The EAE clinical scores in C57BL/6 mice immunized with MOG 35-55 on Day 0 and subsequently injected with 1×10^6 syngeneic GFP-labeled BT-NSCs (filled red triangles; $n = 30$), GPS-treated NSCs (GPS-NSC; filled green circles; $n = 30$) or sham-treated mice (No NSC; filled black circles; $n = 30$) on Days 9 and 13 after immunization were determined. Mice that received GPS-NSCs displayed a pronounced clinical improvement compared with sham-treated mice ($P = 0.0001$) and mice injected i.v. with BT-NSCs ($P = 0.006$). (**B**) The cumulative burden of disease was assessed by performing a linear regression analysis comparing the slope of the curves in (A). These data highlight GPS-NSCs (green dotted line) significantly improve the clinical scores above that of BT-NSCs (red line). Mice receiving either GPS-NSCs or BT-NSCs displayed significantly improved clinical scores compared with mice that did not receive NSCs (No NSCs; black line). These data also suggest that BT-HSPCs (blue line) and GPS-HSPCs (purple line) worsen disease. (**C**) Neuropathology at Day 30 PI of the brain from EAE mice injected with NSCs was analyzed by staining with anti-CD11b mAb (green) and the nuclear label To-Pro3 (blue). GPS-NSC injection leads to significantly less injury per brain section as measured by numeration of CD11b macrophage/microglia from 20 different sections of 3 different spinal cords. Bar graphs depict the numeration of CD11b macrophage/microglia in spinal cord sections per HPF from EAE mice that received No NSC, BT-NSC or GPS-NSC and also the numeration of infiltrates per HPF were calculated based on To-Pro3 staining. White boxes correspond to higher-magnification images. Yellow arrowheads correspond to activated microglia, and white arrows correspond to infiltrates in the meninges (m). Note that the microglia in the No NSC samples are more activated than those found in the BT-NSC and GPS-NSC samples. Also the size of the infiltrates in the meninges is larger in the No NSC samples than in the BT-NSC samples. Scale bars, 100 μm for top panels. Scale bars, 50 μm for bottom panels. (**D**) Neuropathology of the brain from EAE mice injected with NSCs was analyzed by staining 20 different sections of 3 separate brains from mice that either received no NSCs (EAE No NSCs), BT-NSC (EAE BT-NSCs) or GPS-NSC (EAE GPS-NSCs) with CD4 (to measure T cell infiltrations), CNPase (to quantify mature oligodendrocytes), Olig-2 (to measure oligodendroglial differentiation) or SOX-9 (to measure multipotency of neural precursors) (green) and To-Pro3 (blue). GPS-NSC injection lead to significantly less T cell infiltrations, higher numbers of oligodendroglia and preservation of progenitor numbers. (**E**) Bar graphs depict the numeration of CD4 T, CNPase, Olig2 and SOX-9 cells in brain sections per HPF from EAE mice that received No NSC, BT-NSC or GPS-NSC (as outlined in D), indicating that animals that received GPS-NSCs display enhanced neuroprotection of progenitor cells. (**F–I**) GPS-NSC and BT-NSC injection leads to increased axonal regeneration and axonal protection compared with No NSC control as measured by increased GAP-43 (green; $P < 0.001$) staining (F) and by decreased staining with the monoclonal antibody SMI32 (red; $P < 0.001$) (H) as assessed by quantitative confocal imaging of GAP43 pixel intensity in >500 individual measurements. To-Pro3 staining dye was used to detect cell nuclei (blue). (G and H) Based on quantitative confocal imaging of >500 individual measurements of pixel intensity (Imitola et al. 2011), graphical representation of GAP-43 (G) and SMI32 (I) was determined; note that SMI32 patterns (I) demonstrated axonal ovoids in animals with EAE, but reduction in animals injected with NSCs (I) and SMI32 pixel intensity showed a gradual correction of axonal integrity in animals with GPS-NSCs. There is a reduction of axonal ovoid and axonal fragments compared with controls and BT-NSCs as depicted in the cartoon below (I). Scale bar, 100 μm except for SMI32 staining where scale bar, 50 μm.

GPS treatment, PI-PLC and bromelain reactions

The procedure for GPS treatment of murine NSCs was as previously described for MSCs (Sackstein et al. 2008). Briefly, neurospheres were first harvested and dissociated into single cells by incubating with phosphate-buffered saline (PBS)/EDTA (0.02%) for 15 min at 37°C. Cells were then washed with HBSS, counted and resuspended in 60 mU/mL FTVI in HBSS (without Ca^{2+} or Mg^{2+}) containing 20 mM N-2-hydroxyethylpiperazine-N-2-ethane sulfonic acid (HEPES), 0.1% human serum albumin and 1 mM guanosine diphosphate-fucose for 40 min at 37°C. PI-PLC reactions were performed at 37°C using 0.1 U/mL for 1 h. Bromelain reactions were performed at 37°C in HBSS + 2% bovine serum albumin (BSA) + 0.1% bromelain for 1 h.

Flow cytometry

Aliquots of cells (2×10^5 cells) were washed with PBS/2% fetal bovine serum (FBS) and incubated with primary mAbs or with isotype control mAbs (either unconjugated or fluorochrome conjugated). The cells were washed in PBS/2% FBS and, for indirect immunofluorescence, incubated with appropriate secondary fluorochrome-conjugated anti-isotype antibodies. After washing cells, Fluorescein isothiocyanate or PE fluorescence intensity was determined using a Cytomics FC 500 MPL flow cytometer (Beckman Coulter, Inc., Fullerton, CA) or with a BD FACSCanto II cytometer (BD Biosciences, Germany).

Immunoprecipitation studies

Cell lysates of BT-NSC or GPS-NSC were incubated with immunoprecipitating antibodies or with appropriate isotype controls and then incubated with Protein G-agarose. Immunoprecipitates were washed extensively using Buffer A containing 2% NP-40 and 1% SDS. In some experiments, immunoprecipitates were treated with *N*-glycosidase F (New England Biolabs, MA, USA) as previously described (Dimitroff et al. 2001). For western blot analysis, all immunoprecipitates were diluted in reducing sample buffer, boiled, then subjected to SDS-PAGE, transferred to PVDF membrane and immunostained with HECA-452 or E-Ig.

Western blot analysis

BT- and GPS-NSCs were lysed using 2% NP-40 in Buffer A [150 mM NaCl, 50 mM Tris-HCl, pH 7.4, 1 mM EDTA, 20 µg/mL PMSF, 0.02% sodium azide and protease inhibitor cocktail tablet (Roche Molecular Biochemicals IN, USA)]. Western blots of quantified protein lysates or of immunoprecipitated protein were performed under reducing conditions as described previously (Dimitroff et al. 2001). Blots were visualized with chemiluminescence using Lumi-Light Western Blotting Substrate (Roche).

Parallel plate flow chamber adhesion assays

E-selectin binding capacity of BT-NSCs and GPS-NSCs was compared using the parallel plate flow chamber assay (Glycotech; Gaithersburg, MD). NSCs (0.5×10^6 cells/mL, suspended in HBSS/10 mM HEPES/2 mM $CaCl_2$ solution) were perfused over confluent HUVEC monolayers. Initially, the NSCs were allowed to contact the HUVEC monolayer at a shear stress of 0.5 dyne/cm^2, subsequently the flow rate was adjusted to exert shear stress ranging from 0.5 to 30 dynes/cm^2. The number of BT- or GPS-NSCs adherent to the HUVEC monolayer was quantified in the final 15 s interval at shear stress of 0.5, 1, 2, 5, 10, 20 and 30 dynes/cm^2. Each assay was performed at least three times and the values averaged. Control assays were performed by adding 5 mM EDTA to the assay buffer to chelate Ca^{2+} required for selectin binding or treating HUVEC with function-blocking anti-human E-selectin mAb at 37°C for 15 min, prior to use in adhesion assays.

Blot-rolling assay

The blot-rolling assay has been described previously (Dimitroff et al. 2000; Fuhlbrigge et al. 2002; Sackstein and Fuhlbrigge 2006) and here was used to detect selectin binding activity of NSC membrane proteins resolved by SDS-PAGE. Western blots of NSC membrane preparations were stained with anti-CLA (HECA-452) and rendered translucent by immersion in DMEM with 10% glycerol. CHO-E cells were resuspended (5×10^6/mL) in DMEM containing 2 mM $CaCl_2$ and 10% glycerol. The blots were placed under a parallel plate flow chamber, and CHO-E cells were perfused at a physiologically relevant shear stress of 1.0 dyne/cm^2, an adjustment in the volumetric flow rate was made to account for the increase in viscosity due to the presence of 10% glycerol in the flow medium. Molecular weight markers were used as guides to aid placement of the flow chamber over stained bands of interest. The number of interacting cells per square millimeter was tabulated as a function of the molecular weight region and compiled into an adhesion histogram. Nonspecific adhesion was assessed by perfusing CHO-E cell suspensions containing 5 mM EDTA in the flow medium.

Immunization for EAE induction and neural stem cells injection

C57BL/6 NSCs or bone marrow HSPCs (Lineage^{neg}C-kit^{pos}) were either treated with GPS or not, and 1×10^6 cells were injected into the tail-vein of C57BL/6 mice on Days 9 and 13 after immunization (PI) with MOG 35-55 (subcutaneously in the flanks; see details in Supplementary data). EAE was scored in a blinded fashion; the investigator was not involved in the injections and was not aware of the composition of the groups. Details of the grading scale used are outlined in the Supplementary data. BT-NSC, GPS-NSCs, BT-HSPCs or GPS-HSPCs were injected as a cell suspension into the tail-vein of EAE mice in a volume of 0.2 mL of HBSS. Sham-treated mice (No NSCs) injected with HBSS alone were used as a negative control.

Short-term homing studies

BT-NSCs and GPS-NSCs were labeled with 5 mM CFDA-SE (Invitrogen) for 5 min at room temperature in Roswell Park Memorial Institute (RPMI)-1640 containing 10% FBS and injected intravenously into MOG-treated C57BL6 mice on Days 9 and 13 PI. Two million NSCs in a volume of 0.2 mL of HBSS were injected into each mouse on each day. HBSS buffer alone was used to determine background signals. BT-NSCs and GPS-NSCs were also injected into animals that were not immunized with MOG and used to standardize the signals observed in each tissue assayed. Sixteen hours after the second NSC transfer, mice were sacrificed and perfused with 1× PBS without Ca^{2+} and Mg^{2+}. The brain, spinal cord, lymph nodes, spleen, liver and lung were isolated. The brain and the spinal cord were homogenized. Resulting pellets were resuspended in 0.25% Trypsin-EDTA (Invitrogen) and incubated at 37°C for 10 min. The digestion process was stopped using DMEM containing 0.01% SBTI, 0.001% DNase and 0.075% BSA. The lymph nodes, spleen and liver were mechanically dissociated and the resulting single-cell suspensions were assessed for frequencies of CFDA-SE positive cells by flow cytometry in the FL1 channel. Flow cytometric data was analyzed and expressed as percent of CFDA-SE-positive events detected in 200,000 cells scanned within a narrow gate that is set to include NSC. This gate was determined based on mixing cultured NSCs with

suspensions of cells isolated from each tissue tested (brain, spinal cord, lymph node, spleen, liver and lung).

Analysis of NSC migration to CNS

BT-NSCs, GPS-NSCs were labeled with PKH26 dye (Invitrogen) and injected intravenously into MOG-treated C57BL6 mice on Days 9 and 13 PI. One million NSCs in a volume of 0.2 mL of HBSS were injected into each mouse on each day specified. HBSS buffer alone was used to determine background signals. Four days after the second NSC transfer, mice were sacrificed and perfused with 1× PBS without Ca^{2+} and Mg^{2+} and lumbar-sacral spinal cords were harvested. The spinal cord was chosen because in the B6 model, the CNS lesions in the forebrain are very variable in size and location compared with the spinal cords, which possess a more predictable location (lumbosacral region) and also more exuberant pathology (Chitnis et al. 2001; Rasmussen et al. 2007; Wang et al. 2008). For flow cytometric analysis, the spinal cords were then homogenized and the resulting pellets were resuspended in 0.25% Trypsin-EDTA (Invitrogen) and incubated at 37°C for 10 min. The digestion process was stopped using DMEM containing 0.01% SBTI, 0.001% DNase and 0.075% BSA. For histology analysis, the brain and spinal cord were snap-frozen in liquid nitrogen and stored in −80°C until sectioning. The cryostat sections (20 µm) of lumbar-sacral spinal cord or anterior, middle and posterior brain were fixed with 4% paraformaldehyde for 15 min and then stained with antibodies of interest, Blood vessels were visualized by anti-Flk-1 (VEGFR2, Sigma) and NSCs were stained with either anti-sox-2 (Millipore) or visualized by PKH26 dye in red. The spinal cords were then homogenized and the resulting pellets were resuspended in 0.25% Trypsin-EDTA (Invitrogen) and incubated at 37°C for 10 min. The digestion process was stopped using DMEM containing 0.01% SBTI, 0.001% DNase and 0.075% BSA. Blood vessels were visualized by Flk-1 (VEGFR2) staining.

Immunization for EAE induction and NSC/HSPC injection

C57BL/6 NSCs or C57BL/6 HSPCs (Lineage^{neg}C-kit^{pos}) were either treated with GPS or not, and 1×10^6 cells were injected into the tail-vein of C57BL/6 mice on Days 9 and 13 post immunization (PI) with MOG 35-55. MOG 35-55 (M-E-V-G-W-Y-R-S-P-F-S-R-O-V-H-L-Y-R-N-G-K) corresponding to mouse sequence is synthesized by QCB, Inc., Division of BioSource International (Hopkinton, MA), and purified to >99% by HPLC. Mice are immunized subcutaneously in the flanks with 150–200 µg of MOG peptide in 0.1 mL PBS and 0.1 mL CFA containing 0.4 mg *Mycobacterium tuberculosis* (H37Ra, Difco, Detroit, MI) and injected intraperitoneally with 200 ng Pertussis toxin (List Laboratories, Campbell, CA) on the day of immunization and 2 days later. EAE was scored in a blinded fashion; the investigator was not involved in the injections and was not aware of the composition of the groups. The following grade was used: Grade 1, limp tail or isolated weakness of gait without limp tail; Grade 2, partial hind leg paralysis; Grade 3, total hind leg or partial hind and front leg paralysis; Grade 4, total hind leg and partial front leg paralysis and Grade 5, moribund or dead animal. BT-NSC, GPS-NSCs, BT-HSPCs and GPS-HSPCs were injected as a cell suspension into the tail-vein of EAE mice in a volume of 0.2 mL of HBSS. Sham-treated mice (No NSCs) injected with HBSS alone were used as a negative control.

Immunohistologic staining

Mice were perfused with 50 mL normal saline before sacrificing to remove any intravascular peripheral blood mononuclear cells (PBMCs). For confocal imaging animals were perfused intracardially with 10 mL of 4% paraformaldehyde in PBS. The brain and the spinal cord were removed and embedded in optimal cutting temperature compound, quick frozen in liquid nitrogen and kept at −70°C until sectioning. Cryostat sections (10 µm) of spinal cords were fixed with acetone or 4% paraformaldehyde and then labeled with the antibody of interest. Isotype-matched Ig and omission of the primary antibody served as negative controls. Each specimen was evaluated at a minimum of three different levels of sectioning. The entire tissue section (a longitudinal spinal cord section) was evaluated for a given cellular marker at 40× magnification. The number of cells staining positive for the given markers was counted in ten 40× [high-power fields (HPFs)] fields per section. The results for one section were totaled, and the results between sections were averaged.

Staining for confocal microscopy

Paraformaldehyde-fixed sections (40 µm) were washed in PBS; blocked in PBS containing 4% goat serum, 0.3% BSA and 0.3% triton; and subsequently incubated with primary antibodies overnight and secondary antibodies for 2 h in blocking solution. We used highly cross-adsorbed secondary antibodies to avoid cross-reactivity (Alexa 488 and Alexa 594). Confocal microscopy was performed using a Zeiss Laser Scanning Microscope 3D analysis software (Zeiss, Thornwood, NY) with a multitrack acquisition protocol to avoid potential overlapping of the two fluorochromes.

Effects of GPS treatment on NSC differentiation, self-renewal capacity and immunosuppressive effects in vitro

The procedure for GPS treatment of murine NSCs was as previously described for MSCs (Sackstein et al. 2008). BT- and GPS-NSCs were compared in vitro for their capacity to self-renew, form neurospheres, differentiate into MAP2$^+$ neurons and inhibit the proliferation of ConA activated lymph node cells. *NSC differentiation and self-renewal capacity*: Neurospheres initially cultured in FGF/EGF containing media were plated on poly-D-lysine (PDL)-coated glass coverslips allowed to proliferate then harvested and treated for an hour with buffer (control) or enzymatic treatment with FTVI (60 mU/mL), subsequently the resulting BT-NSCs and GPS-NSCs were plated at clonal density of 20 cells per µL and allowed to proliferate as neurospheres for 96 h to 5 days. Neurosphere imaging was captured with an Axiovision microscope (NY, USA). For neuronal, astrocyte and oligodendrocyte differentiation, dissociated neurospheres were plated on PL-coated glass coverslips in a 24-well plate and cultured without FGF/EGF but in the presence of neurobasal medium containing 1% glutamax, 1% antibiotic/antimycotic and 2% B27 supplement. Fresh media was added every other day until Day 5, and the cells were then subjected to immunofluorescence staining with MAP2 (neurons), GFAP (astrocytes) and NG2 (oligodendrocyte precursors). MAP2$^+$, GFAP$^+$ and NG2$^+$ cells were counted using standard stereological technique by an investigator blinded to the treatments. *Co-cultures of Neural Stem Cells and Lymph Node Cells*: Lymph nodes were isolated from naïve C57BL/6 mice. Lymph node cells (LNCs) were cultured as single-cell suspensions in a 96-well plate at 2×10^5 cells per well, as previously described (Einstein et al. 2007). Culture medium consisted of RPMI-1640 supplemented with 10% FBS, L-glutamine, sodium pyruvate, nonessential amino acid, 2-mercaptoethanol, HEPES and antibiotics (BioWhittaker, MD, USA) with 2.5 µg/mL concanavalin A (ConA, Sigma) or without. Neurospheres were dissociated and were first either treated with GPS or not (BT) and subsequently irradiated with 3000 Rad. Following irradiation, the dissociated NSCs were then added directly to the LNC culture medium at different ratios with ConA

stimulated LNCs. The ratios tested of numbers of NSCs to numbers of LNCs were 1:4, 1:2, 1:1, 2:1 and 4:1. The cells were then cultured for 48 h before adding thymidine. Thymidine incorporation assays were performed 16 h later.

Assessment of E-selectin ligands following treatment of NSCs with inflammatory cytokines

About 1.5×10^6 cells/well were seeded in a six-well plate containing 3 mL proliferation medium per well and stimulated with either 10 ng/mL of TNF-α (R&D; 410-TRNC), 10 ng/mL IL-1β (R&D; 401-ML) and 10 ng/mL IFNγ (R&D; 485-MI) independently or in combination (all three at 10 ng/mL). After 24 and 48 h, the neurospheres were harvested by centrifugation and stained with E-Ig for flow cytometric analysis.

Measurement of LIF mRNA

About 1×10^6 mouse embryonic NSCs were treated for 24 h with or without inflammatory cytokines (IFN-ϒ at 10 ng/mL and TNF-α at 15 ng/mL). Total RNA was then extracted using Trizol reagent, and the quality of the extracted RNA was measured using Agilent 2200 Tab station system. cDNA synthesis was done using high-capacity cDNA reverse transcription kit (Applied Biosystems) and a Random Hexamer. mRNA level was measured using reverse transcriptase-polymerase chain reaction (RT-PCR), and the fold change in gene expression was calculated using $2^{-\Delta\Delta CT}$ method. The forward primer sequence for the LIF gene was CCTACCTGCGTCTTACTCCATCA and the reverse primer was CCCCAAAGGCTCAATGGTT (Sigma). The relative expression of LIF mRNA was assayed relative to glyceraldehyde 3-phosphate dehydrogenase housekeeping gene in which TGCAC CACCAACTGCTTAGC was used as a forward primer and GGCATG GACTGTGGTCATGAG as reverse primer.

Analysis of NSC migration to CNS

BT-NSCs and GPS-NSCs were labeled with PKH26 dye (Invitrogen) and injected intravenously into MOG-treated C57BL6 mice on Days 9 and 13 PI. One million NSCs were injected into each mouse on each day. HBSS buffer alone was used to determine background signals. Either 24 h or 4 days after the second NSC transfer, mice were sacrificed, perfused and lumbar-sacral spinal cords were harvested. The spinal cord was chosen because in the B6 model, the CNS lesions in the forebrain are very variable in size and location compared with the spinal cords, which possess a more predictable location (lumbosacral region) and also more exuberant pathology (Chitnis et al. 2001; Rasmussen et al. 2007; Wang et al. 2008). For flow cytometric analysis, the spinal cords were then homogenized and the resulting pellets were resuspended in 0.25% Trypsin-EDTA and incubated at 37°C for 10 min. The digestion process was stopped using DMEM containing 0.01% SBTI, 0.001% DNase and 0.075% BSA. For histology analysis, the brain and the spinal cord were snap-frozen in liquid nitrogen and stored in −80°C until sectioning. The cryostat sections (20 µm) of lumbar-sacral spinal cord or anterior, middle and posterior brain were fixed and then stained with antibodies of interest. Blood vessels were visualized by anti-Flk-1 (VEGFR2), and NSCs were stained with either anti-SOX-2 or visualized by PKH26 dye in red. For neuropathology analysis, cell quantification was performed by stereological analysis of animals in different groups. The spinal cords and the brain were sectioned, and every third section of the cervical and lumbosacral region was stained; cell quantification was performed in high-power magnification of 3–5 sections. LSM 510 Confocal microscope with motorized stage was used to stereologically calculate the intensity of staining and total cell numbers per high-power magnification.

Statistical analysis

Data are expressed as the mean ± SEM. Statistical significance of differences between means was determined by two-way ANalysis Of VAriance (ANOVA). If means were shown to be significantly different, multiple comparisons were performed post hoc by the Turkey *t*-test. Statistical significance was defined as $P < 0.05$.

Supplementary data

Supplementary data for this article are available online at http://glycob.oxfordjournals.org/.

Authors' contributions

R.S.: Concept and design (developed critical reagents), financial support, data analysis and interpretation, manuscript writing, final approval of manuscript. S.J.K.: concept and design, financial support, data analysis and interpretation, final approval of manuscript. J.S.M.: concept and design, collection and assembly of data, data analysis and interpretation, manuscript writing. J.I.: concept and design, collection and assembly of data, data analysis and interpretation, manuscript writing. S.C.S.: collection and assembly of data, data analysis and interpretation. B.Z.: collection and assembly of data, data analysis and interpretation. Y.W.: collection and assembly of data, data analysis and interpretation. J.L.: collection and assembly of data, data analysis and interpretation. A.J.A.: collection and assembly of data, data analysis and interpretation. M.O.: collection and assembly of data, data analysis and interpretation. A.F.A.: assembly of data, data analysis and interpretation.

Funding

This effort was supported by National Institutes of Health grants PO1 HL107146 [NHLBI Program of Excellence in Glycosciences (R.S.)], RO1 HL73714 (R.S.), RO1 HL60528 (R.S.), AI043496 (S.J.K.) and AI071448 (S.J.K.). This work was also supported by the Edward and Dana Slatkin Research Fund and the Brourman Family Fund (R.S.), and by a National Multiple Sclerosis Society grant RG3945 (S.J.K). The King Abdullah University of Science and Technology Faculty Baseline Research Funding Program (J.S.M.) also supported this work. The funders had no role in study design, data collection and analysis, decision to publish or preparation of the manuscript.

Acknowledgements

We thank E. Grady and J.K. Kennedy for skilled technical support. We would also like to thank Dr. Kosuke Sakashita for his technical expertise.

Conflict of interest

In accordance with National Institutes of Health policies and procedures, the Brigham & Women's Hospital has assigned intellectual property rights regarding HCELL and GPS to the inventor (R.S.), who may benefit financially if the technology is licensed. R.S.'s ownership interests were reviewed and are managed by the Brigham & Women's Hospital and Partners HealthCare in accordance with their conflict of interest policy.

Abbreviations

ANOVA, ANalysis Of VAriance (ANOVA); BT, buffer treated; CHO, Chinese hamster ovary; CLA, cutaneous lymphocyte antigen (CLA); CNS, central nervous system; ConA, conconavalin A; E-Ig, E-selectin-Ig chimera; EAE, experimental autoimmune encephalomyelitis; EDTA, ethylenediaminetetraacetic acid; GPI, glycophosphatidylinositol; GPS, glycosyltransferase-programmed stereosubstitution; HBSS, hank's balanced salt solution (HBSS); HCELL, hematopoietic cell E-/L-selectin ligand; HEPES, N-2-hydroxyethylpiperazine-N-2-ethane sulfonic acid (HEPES); HSPC, hematopoietic stem/progenitor cells; HUVEC, human umbilical vein endothelial cells; i.v., intravenously (i.v.); IFN-γ, interferon gamma; LeX, Lewis X; LIF, leukemia inhibitory factor; mAb, monoclonal antibody; MOG, myelin oligodendrocyte glycoprotein (MOG); NCAM, neural cell adhesion molecule; NSC, neural stem cell; P-Ig, P-selectin-Ig chimera; PE, phycoerythrin (PE); PI-PLC, phosphatidylinositol phospholipase C; PI, post-immunization; PNGaseF, N-glycosidase F; PSA, poly sialic acid; RPMI, Roswell Park Memorial Institute (RPMI); SBTI, soybean trypsin inhibitor (SBTI); SDS-PAGE, sodium dodecyl sulfate-polyacrylamide gel electrophoresis; sLeX, Sialyl Lewis X; TNF-α, tumor necrosis factor alpha; VCAM-1, vascular cell adhesion molecule 1; VLA-4, very late antigen 4.

References

AbuSamra DB, Al-Kilani A, Hamdan SM, Sakashita K, Gadhoum SZ, Merzaban JS. 2015. Quantitative characterization of E-selectin interaction with native CD44 and P-selectin glycoprotein ligand-1 (PSGL-1) using a real-time immunoprecipitation-based binding assay. *J Biol Chem*. 290:21213–21230.

Alam HB, Sun L, Ruff P, Austin B, Burris D, Rhee P. 2000. E- and P-selectin expression depends on the resuscitation fluid used in hemorrhaged rats. *The Journal of Surgical Research*. 94:145–152.

Alon R, Feizi T, Yuen CT, Fuhlbrigge RC, Springer TA. 1995. Glycolipid ligands for selectins support leukocyte tethering and rolling under physiologic flow conditions. *Journal of Immunology*. 154:5356–5366.

Back SA, Tuohy TM, Chen H, Wallingford N, Craig A, Struve J, Luo NL, Banine F, Liu Y, Chang A, et al. 2005. Hyaluronan accumulates in demyelinated lesions and inhibits oligodendrocyte progenitor maturation. *Nature Medicine*. 11:966–972.

Ben-Hur T, Einstein O, Mizrachi-Kol R, Ben-Menachem O, Reinhartz E, Karussis D, Abramsky O. 2003. Transplanted multipotential neural precursor cells migrate into the inflamed white matter in response to experimental autoimmune encephalomyelitis. *Glia*. 41:73–80.

Berlin C, Bargatze RF, Campbell JJ, von Andrian UH, Szabo MC, Hasslen SR, Nelson RD, Berg EL, Erlandsen SL, Butcher EC. 1995. Alpha 4 integrins mediate lymphocyte attachment and rolling under physiologic flow. *Cell*. 80:413–422.

Bezzi P, Domercq M, Brambilla L, Galli R, Schols D, De Clercq E, Vescovi A, Bagetta G, Kollias G, Meldolesi J, et al. 2001. CXCR4-activated astrocyte glutamate release via TNFalpha: Amplification by microglia triggers neurotoxicity. *Nature Neuroscience*. 4:702–710.

Butcher EC. 1991. Leukocyte-endothelial cell recognition: Three (or more) steps to specificity and diversity. *Cell*. 67:1033–1036.

Campos LS, Decker L, Taylor V, Skarnes W. 2006. Notch, epidermal growth factor receptor, and beta1-integrin pathways are coordinated in neural stem cells. *The Journal of Biological Chemistry*. 281:5300–5309.

Campos LS, Leone DP, Relvas JB, Brakebusch C, Fassler R, Suter U, ffrench-Constant C. 2004. Beta1 integrins activate a MAPK signalling pathway in neural stem cells that contributes to their maintenance. *Development*. 131:3433–3444.

Caplan AI. 2009. Why are MSCs therapeutic? New data: New insight. *The Journal of Pathology*. 217:318–324.

Chitnis T, Najafian N, Abdallah KA, Dong V, Yagita H, Sayegh MH, Khoury SJ. 2001. CD28-independent induction of experimental autoimmune encephalomyelitis. *J Clin Invest*. 107:575–583.

Deboux C, Ladraa S, Cazaubon S, Ghribi-Mallah S, Weiss N, Chaverot N, Couraud PO, Baron-Van Evercooren A. 2013. Overexpression of CD44 in neural precursor cells improves trans-endothelial migration and facilitates their invasion of perivascular tissues in vivo. *PloS One*. 8:e57430.

Dimitroff CJ, Lee JY, Fuhlbrigge RC, Sackstein R. 2000. A distinct glycoform of CD44 is an L-selectin ligand on human hematopoietic cells. *Proceedings of the National Academy of Sciences of the United States of America*. 97:13841–13846.

Dimitroff CJ, Lee JY, Rafii S, Fuhlbrigge RC, Sackstein R. 2001. CD44 is a major E-selectin ligand on human hematopoietic progenitor cells. *J Cell Biol*. 153:1277–1286.

Ding ZM, Babensee JE, Simon SI, Lu H, Perrard JL, Bullard DC, Dai XY, Bromley SK, Dustin ML, Entman ML, et al. 1999. Relative contribution of LFA-1 and Mac-1 to neutrophil adhesion and migration. *Journal of Immunology*. 163:5029–5038.

Drake TA, Cheng J, Chang A, Taylor FB Jr 1993. Expression of tissue factor, thrombomodulin, and E-selectin in baboons with lethal Escherichia coli sepsis. *The American Journal of Pathology*. 142:1458–1470.

Einstein O, Fainstein N, Vaknin I, Mizrachi-Kol R, Reihartz E, Grigoriadis N, Lavon I, Baniyash M, Lassmann H, Ben-Hur T. 2007. Neural precursors attenuate autoimmune encephalomyelitis by peripheral immunosuppression. *Annals of Neurology*. 61:209–218.

Einstein O, Grigoriadis N, Mizrachi-Kol R, Reinhartz E, Polyzoidou E, Lavon I, Milonas I, Karussis D, Abramsky O, Ben-Hur T. 2006. Transplanted neural precursor cells reduce brain inflammation to attenuate chronic experimental autoimmune encephalomyelitis. *Experimental Neurology*. 198:275–284.

Emamgholipour S, Eshaghi SM, Hossein-nezhad A, Mirzaei K, Maghbooli Z, Sahraian MA. 2013. Adipocytokine profile, cytokine levels and foxp3 expression in multiple sclerosis: A possible link to susceptibility and clinical course of disease. *PloS One*. 8:e76555.

Flax JD, Aurora S, Yang C, Simonin C, Wills AM, Billinghurst LL, Jendoubi M, Sidman RL, Wolfe JH, Kim SU, et al. 1998. Engraftable human neural stem cells respond to developmental cues, replace neurons, and express foreign genes. *Nat Biotechnol*. 16:1033–1039.

Fu J, Yang QY, Sai K, Chen FR, Pang JC, Ng HK, Kwan AL, Chen ZP. 2013. TGM2 inhibition attenuates ID1 expression in CD44-high glioma-initiating cells. *Neuro-oncology*. 15:1353–1365.

Fuhlbrigge RC, Kieffer JD, Armerding D, Kupper TS. 1997. Cutaneous lymphocyte antigen is a specialized form of PSGL-1 expressed on skin-homing T cells. *Nature*. 389:978–981.

Fuhlbrigge RC, King SL, Dimitroff CJ, Kupper TS, Sackstein R. 2002. Direct real-time observation of E- and P-selectin-mediated rolling on cutaneous lymphocyte-associated antigen immobilized on western blots. *Journal of Immunology*. 168:5645–5651.

Gadhoum SZ, Sackstein R. 2008. CD15 expression in human myeloid cell differentiation is regulated by sialidase activity. *Nat Chem Biol*. 4:751–757.

Gascon E, Vutskits L, Kiss JZ. 2007. Polysialic acid-neural cell adhesion molecule in brain plasticity: From synapses to integration of new neurons. *Brain Res Rev*. 56:101–118.

Glaser T, Brose C, Franceschini I, Hamann K, Smorodchenko A, Zipp F, Dubois-Dalcq M, Brustle O. 2007. Neural cell adhesion molecule polysialylation enhances the sensitivity of embryonic stem cell-derived neural precursors to migration guidance cues. *Stem Cells*. 25:3016–3025.

Goncharova V, Das S, Niles W, Schraufstatter I, Wong AK, Povaly T, Wakeman D, Miller L, Snyder EY, Khaldoyanidi SK. 2014. Homing of neural stem cells from the venous compartment into a brain infarct does not involve conventional interactions with vascular endothelium. *Stem Cells Translational Medicine*. 3:229–240.

Hess DC, Borlongan CV. 2008. Stem cells and neurological diseases. *Cell Proliferation*. 41 Suppl 1:94–114.

Horie K, Sakagami M, Kuramochi K, Ito T, Hamana H. 2000. Effect of the sialyl Lewis X (SLe(x)) moiety on splenic accumulation of SLe(x)-carboxymethylpullulan conjugate. *Microbiology and Immunology*. 44:401–404.

Horie K, Sakagami M, Masuda K, Notoya M, Hamana H, Yoshikawa T, Hirano K. 2004. Sialyl Lewis X-carboxymethylpullulan conjugate: A novel homing device to spleen and lymph nodes. *Biological & Pharmaceutical Bulletin*. 27:1275–1280.

Imitola J, Chitnis T, Khoury SJ. 2006. Insights into the molecular pathogenesis of progression in multiple sclerosis: Potential implications for future therapies. *Arch Neurol*. 63:25–33.

Imitola J, Comabella M, Chandraker AK, Dangond F, Sayegh MH, Snyder EY, Khoury SJ. 2004. Neural stem/progenitor cells express costimulatory molecules that are differentially regulated by inflammatory and apoptotic stimuli. *The American Journal of Pathology*. 164:1615–1625.

Imitola J, Cote D, Rasmussen S, Xie XS, Liu Y, Chitnis T, Sidman RL, Lin CP, Khoury SJ. 2011. Multimodal coherent anti-Stokes Raman scattering microscopy reveals microglia-associated myelin and axonal dysfunction in multiple sclerosis-like lesions in mice. *Journal of Biomedical Optics*. 16:021109.

Imitola J, Raddassi K, Park KI, Mueller FJ, Nieto M, Teng YD, Frenkel D, Li J, Sidman RL, Walsh CA, et al. 2004. Directed migration of neural stem cells to sites of CNS injury by the stromal cell-derived factor 1alpha/CXC chemokine receptor 4 pathway. *Proceedings of the National Academy of Sciences of the United States of America*. 101:18117–18122.

Ji JF, He BP, Dheen ST, Tay SS. 2004. Expression of chemokine receptors CXCR4, CCR2, CCR5 and CX3CR1 in neural progenitor cells isolated from the subventricular zone of the adult rat brain. *Neuroscience Letters*. 355:236–240.

Justicia C, Martin A, Rojas S, Gironella M, Cervera A, Panes J, Chamorro A, Planas AM. 2006. Anti-VCAM-1 antibodies did not protect against ischemic damage either in rats or in mice. *J Cereb Blood Flow Metab*. 26:421–432.

Kumar A, Torii T, Ishino Y, Muraoka D, Yoshimura T, Togayachi A, Narimatsu H, Ikenaka K, Hitoshi S. 2013. The Lewis X-related alpha1, 3-fucosyltransferase, Fut10, is required for the maintenance of stem cell populations. *The Journal of Biological Chemistry*. 288:28859–28868.

Laterza C, Merlini A, De Feo D, Ruffini F, Menon R, Onorati M, Fredrickx E, Muzio L, Lombardo A, Comi G, et al. 2013. iPSC-derived neural precursors exert a neuroprotective role in immune-mediated demyelination via the secretion of LIF. *Nature Communications*. 4:2597.

Lavdas AA, Franceschini I, Dubois-Dalcq M, Matsas R. 2006. Schwann cells genetically engineered to express PSA show enhanced migratory potential without impairment of their myelinating ability in vitro. *Glia*. 53:868–878.

Lee SJ, Benveniste EN. 1999. Adhesion molecule expression and regulation on cells of the central nervous system. *Journal of Neuroimmunology*. 98:77–88.

Lee ST, Chu K, Jung KH, Kim SJ, Kim DH, Kang KM, Hong NH, Kim JH, Ban JJ, Park HK, et al. 2008. Anti-inflammatory mechanism of intravascular neural stem cell transplantation in haemorrhagic stroke. *Brain: A Journal of Neurology*. 131:616–629.

Leone DP, Relvas JB, Campos LS, Hemmi S, Brakebusch C, Fassler R, Ffrench-Constant C, Suter U. 2005. Regulation of neural progenitor proliferation and survival by beta1 integrins. *J Cell Sci*. 118:2589–2599.

Leppanen A, White SP, Helin J, McEver RP, Cummings RD. 2000. Binding of glycosulfopeptides to P-selectin requires stereospecific contributions of individual tyrosine sulfate and sugar residues. *The Journal of Biological Chemistry*. 275:39569–39578.

Liu H, Zhang J, Liu CY, Wang IJ, Sieber M, Chang J, Jester JV, Kao WW. 2010. Cell therapy of congenital corneal diseases with umbilical mesenchymal stem cells: Lumican null mice. *PloS One*. 5:e10707.

Maness PF, Schachner M. 2007. Neural recognition molecules of the immunoglobulin superfamily: Signaling transducers of axon guidance and neuronal migration. *Nature Neuroscience*. 10:19–26.

Martino G, Pluchino S. 2006. The therapeutic potential of neural stem cells. *Nat Rev Neurosci*. 7:395–406.

Merzaban JS, Burdick MM, Gadhoum SZ, Dagia NM, Chu JT, Fuhlbrigge RC, Sackstein R. 2011. Analysis of glycoprotein E-selectin ligands on human and mouse marrow cells enriched for hematopoietic stem/progenitor cells. *Blood*. 118:1774–1783.

Mollicone R, Moore SE, Bovin N, Garcia-Rosasco M, Candelier JJ, Martinez-Duncker I, Oriol R. 2009. Activity, splice variants, conserved peptide motifs, and phylogeny of two new alpha1,3-fucosyltransferase families (FUT10 and FUT11). *The Journal of Biological Chemistry*. 284:4723–4738.

Phinney DG, Prockop DJ. 2007. Concise review: Mesenchymal stem/multipotent stromal cells: The state of transdifferentiation and modes of tissue repair—current views. *Stem cells (Dayton, Ohio)*. 25:2896–2902.

Piccio L, Rossi B, Colantonio L, Grenningloh R, Gho A, Ottoboni L, Homeister JW, Scarpini E, Martinello M, Laudanna C, et al. 2005. Efficient recruitment of lymphocytes in inflamed brain venules requires expression of cutaneous lymphocyte antigen and fucosyltransferase-VII. *Journal of Immunology*. 174:5805–5813.

Piccio L, Rossi B, Scarpini E, Laudanna C, Giagulli C, Issekutz AC, Vestweber D, Butcher EC, Constantin G. 2002. Molecular mechanisms involved in lymphocyte recruitment in inflamed brain microvessels: Critical roles for P-selectin glycoprotein ligand-1 and heterotrimeric G(i)-linked receptors. *Journal of Immunology*. 168:1940–1949.

Pluchino S, Quattrini A, Brambilla E, Gritti A, Salani G, Dina G, Galli R, Del Carro U, Amadio S, Bergami A, et al. 2003. Injection of adult neurospheres induces recovery in a chronic model of multiple sclerosis. *Nature*. 422:688–694.

Pluchino S, Zanotti L, Brini E, Ferrari S, Martino G. 2009. Regeneration and repair in multiple sclerosis: The role of cell transplantation. *Neuroscience Letters*. 456:101–106.

Pluchino S, Zanotti L, Rossi B, Brambilla E, Ottoboni L, Salani G, Martinello M, Cattalini A, Bergami A, Furlan R, et al. 2005. Neurosphere-derived multipotent precursors promote neuroprotection by an immunomodulatory mechanism. *Nature*. 436:266–271.

Politi LS, Bacigaluppi M, Brambilla E, Cadioli M, Falini A, Comi G, Scotti G, Martino G, Pluchino S. 2007. Magnetic-resonance-based tracking and quantification of intravenously injected neural stem cell accumulation in the brains of mice with experimental multiple sclerosis. *Stem Cells*. 25:2583–2592.

Polley MJ, Phillips ML, Wayner E, Nudelman E, Singhal AK, Hakomori S, Paulson JC. 1991. CD62 and endothelial cell-leukocyte adhesion molecule 1 (ELAM-1) recognize the same carbohydrate ligand, sialyl-Lewis x. *Proceedings of the National Academy of Sciences of the United States of America*. 88:6224–6228.

Rampon C, Weiss N, Deboux C, Chaverot N, Miller F, Buchet D, Tricoire-Leignel H, Cazaubon S, Baron-Van Evercooren A, Couraud PO. 2008. Molecular mechanism of systemic delivery of neural precursor cells to the brain: Assembly of brain endothelial apical cups and control of transmigration by CD44. *Stem Cells*. 26:1673–1682.

Rasmussen S, Wang Y, Kivisakk P, Bronson RT, Meyer M, Imitola J, Khoury SJ. 2007. Persistent activation of microglia is associated with neuronal dysfunction of callosal projecting pathways and multiple sclerosis-like lesions in relapsing—remitting experimental autoimmune encephalomyelitis. *Brain: A Journal of Neurology*. 130:2816–2829.

Redl H, Dinges HP, Buurman WA, van der Linden CJ, Pober JS, Cotran RS, Schlag G. 1991. Expression of endothelial leukocyte adhesion molecule-1 in septic but not traumatic/hypovolemic shock in the baboon. *The American Journal of Pathology*. 139:461–466.

Rosen SD. 2004. Ligands for L-selectin: Homing, inflammation, and beyond. *Annu Rev Immunol*. 22:129–156.

Rutishauser U. 2008. Polysialic acid in the plasticity of the developing and adult vertebrate nervous system. *Nat Rev Neurosci*. 9:26–35.

Sackstein R. 2004. The bone marrow is akin to skin: HCELL and the biology of hematopoietic stem cell homing. *J Invest Dermatol*. 122:1061–1069.

Sackstein R. 2005. The lymphocyte homing receptors: Gatekeepers of the multistep paradigm. *Curr Opin Hematol*. 12:444–450.

Sackstein R, Fuhlbrigge R. 2006. The blot rolling assay: A method for identifying adhesion molecules mediating binding under shear conditions. *Methods in Molecular Biology*. 341:217–226.

Sackstein R, Merzaban JS, Cain DW, Dagia NM, Spencer JA, Lin CP, Wohlgemuth R. 2008. Ex vivo glycan engineering of CD44 programs human multipotent mesenchymal stromal cell trafficking to bone. *Nature Medicine*. 14:181–187.

Schweitzer KM, Drager AM, van der Valk P, Thijsen SF, Zevenbergen A, Theijsmeijer AP, van der Schoot CE, Langenhuijsen MM. 1996. Constitutive expression of E-selectin and vascular cell adhesion molecule-1 on endothelial cells of hematopoietic tissues. *The American Journal of Pathology*. 148:165–175.

Springer TA. 1994. Traffic signals for lymphocyte recirculation and leukocyte emigration: The multistep paradigm. *Cell*. 76:301–314.

Vitry S, Avellana-Adalid V, Lachapelle F, Evercooren AB. 2001. Migration and multipotentiality of PSA-NCAM+ neural precursors transplanted in the developing brain. *Molecular and Cellular Neurosciences*. 17:983–1000.

Wang Y, Imitola J, Rasmussen S, O'Connor KC, Khoury SJ. 2008. Paradoxical dysregulation of the neural stem cell pathway sonic hedgehog-Gli1 in autoimmune encephalomyelitis and multiple sclerosis. *Annals of Neurology*. 64:417–427.

Wang L, Shi J, van Ginkel FW, Lan L, Niemeyer G, Martin DR, Snyder EY, Cox NR. 2009. Neural stem/progenitor cells modulate immune responses by suppressing T lymphocytes with nitric oxide and prostaglandin E2. *Experimental Neurology*. 216:177–183.

Washington R, Burton J, Todd RF 3rd, Newman W, Dragovic L, Dore-Duffy P. 1994. Expression of immunologically relevant endothelial cell activation antigens on isolated central nervous system microvessels from patients with multiple sclerosis. *Annals of Neurology*. 35:89–97.

Weishaupt A, Jander S, Bruck W, Kuhlmann T, Stienekemeier M, Hartung T, Toyka KV, Stoll G, Gold R. 2000. Molecular mechanisms of high-dose antigen therapy in experimental autoimmune encephalomyelitis: Rapid induction of Th1-type cytokines and inducible nitric oxide synthase. *Journal of Immunology*. 165:7157–7163.

Zarbock A, Kempf T, Wollert KC, Vestweber D. 2012. Leukocyte integrin activation and deactivation: Novel mechanisms of balancing inflammation. *Journal of Molecular Medicine*. 90:353–359.

Zarbock A, Lowell CA, Ley K. 2007. Spleen tyrosine kinase Syk is necessary for E-selectin-induced alpha(L)beta(2) integrin-mediated rolling on intercellular adhesion molecule-1. *Immunity*. 26:773–783.

Zhang H, Vutskits L, Calaora V, Durbec P, Kiss JZ. 2004. A role for the polysialic acid-neural cell adhesion molecule in PDGF-induced chemotaxis of oligodendrocyte precursor cells. *J Cell Sci*. 117:93–103.

Ziv Y, Avidan H, Pluchino S, Martino G, Schwartz M. 2006. Synergy between immune cells and adult neural stem/progenitor cells promotes functional recovery from spinal cord injury. *Proceedings of the National Academy of Sciences of the United States of America*. 103:13174–13179.